K.L. Tanaka and W.K. Hartmann

Chapter 15

The Planetary Time Scale

Abstract: Formal stratigraphic systems have been developed for the surface materials of Earth's Moon, Mars, and Mercury. The systems are based on regional and global geologic mapping, which establishes relative ages of surfaces delineated by superposition, morphology, impact crater densities, and other relations and features. Referent units selected from the mapping determine time-stratigraphic bases and/or representative materials characteristic of events and periods for definition of chronologic units. Approximate absolute ages of these units in most cases can be established using crater size-frequency data. For the Moon, the chronologic units and cratering record are calibrated by radiometric ages measured from samples collected from the lunar surface by the Apollo and Luna missions. Model ages for other cratered planetary surfaces are constructed by two methods: (1) estimating relative cratering rates with Earth's Moon, and (2) estimating cratering rates directly based on surveys of the sizes and trajectories of asteroids and comets. Other cratered bodies with estimated surface ages include Venus and the Galilean satellites of Jupiter.

Chapter Outline

15.1. Introduction and Methodologies **275**
15.2. Time Scales **277**
15.2.1. Earth's Moon 277
15.2.1.1. Pre-Nectarian Period 282
15.2.1.2. Nectarian Period 282
15.2.1.3. Early Imbrian Epoch 283
15.2.1.4. Late Imbrian Epoch 283
15.2.1.5. Eratosthenian Period 283
15.2.1.6. Copernican Period 284
15.2.2. Mars 284
15.2.2.1. Pre-Noachian Period 287
15.2.2.2. Early Noachian Epoch 287
15.2.2.3. Middle Noachian Epoch 288
15.2.2.4. Late Noachian Epoch 288
15.2.2.5. Early Hesperian Epoch 288
15.2.2.6. Late Hesperian Epoch 289
15.2.2.7. Early Amazonian Epoch 290
15.2.2.8. Middle Amazonian Epoch 290
15.2.2.9. Late Amazonian Epoch 291
15.2.3. Mercury 291
15.2.4. Venus 293
15.2.5. Other Cratered Bodies 293
References **294**

15.1. INTRODUCTION AND METHODOLOGIES

Stratigraphic studies of solid planetary surfaces residing within our solar system but outside of Earth have led to awareness that each planetary body or satellite has a unique geological record, yet all share membership of a family of objects that are evolving together. That shared history particularly involves the interaction of these larger bodies with populations of smaller objects transiting the solar system, including meteoroids, asteroids, and comets. These objects were especially abundant during earlier solar system evolution, resulting in a record of impact craters preserved on most solid planetary surfaces. Once it became widely accepted that the craters on the Moon were mostly the result of impacts, the cratering record became a quantitative means for independently determining and constraining the relative ages of geologic surfaces and features. As an example of the strength of the method, Hartmann (1965) used statistics of the then newly discovered Canadian impact craters to derive correctly, prior to the Apollo missions, an age for the lunar lava plains. Numbers of large eroded impact craters in several provinces of the Canadian shield were divided by the area and age of those provinces to give an estimated crater formation rate in the Earth–Moon system averaging over a time span of roughly the last billion years. The conclusion of that paper was that "comparison with crater counts on the Moon gives an age of about 3.6 [Ga] for the lunar maria". This estimate turned out to be quite accurate. This suggests that the simple technique of measuring crater densities on relatively homogeneous geological formations provides a fundamental

The Geologic Time Scale 2012. DOI: 10.1016/B978-0-444-59425-9.00015-9

framework that enables the determination of at least approximate time scales for the planetary surfaces of the inner solar system, including Earth's Moon, Mars, Mercury, and Venus. Clearly, there are additional challenges in applying the system to other planets. For example, until we have ground-truth calibration from a few sites on each planet, we must deal with uncertainties of scaling from the current measurements of impact rates on the Moon (and decameter-scale impact rates on Mars) to impact rates on other planets. In principle, however, the system will have further application in estimating chronologies of geological formations where we do not yet have samples for radiometric dating.

The space-age era of lunar research produced the underpinnings for the planetary time scale. High-resolution imaging from orbiting spacecraft enabled complete photogeologic mapping of Earth's Moon. The mapping in turn provided the basis for the construction of a formal stratigraphy, built upon major impact and volcanic resurfacing events used to demarcate periods of geologic activity. Returned rock samples of key units in the stratigraphic record permitted determination of radiometric ages useful for calibrating age vs. crater density (Figure 15.1), and constraining the chronology of the stratigraphic unit boundaries. Such data reveal the mean cratering rate over the past 3 or 3.5 Ga. More recently, telescopic surveys have counted and measured the sizes, trajectories, and velocities of asteroids and comets directly, enabling quantitative estimates of modern cratering rates for the Earth–Moon system and beyond.

Establishment of a lunar chronology led to estimates of its cratering rate history. Theoretical arguments, along with observations of impactor populations and studies of their dynamics, are used to model cratering rates of other planetary

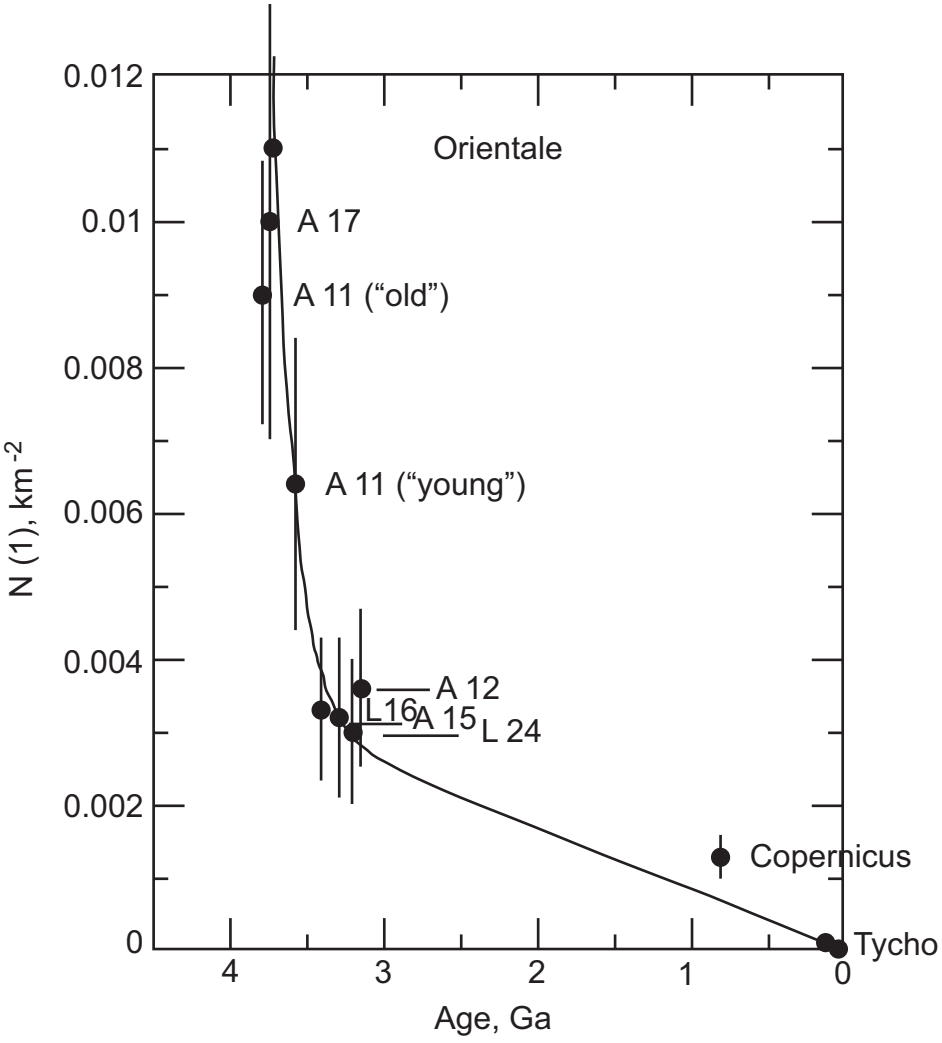

FIGURE 15.1 Crater density vs. age for lunar sites with measured or estimated ages (see text for discussion). This plot is made with a linear scale in crater density. Crater density is expressed here in terms of N(1) = number of craters of D >1 km, per square km. The figure demonstrates that the crater production rate was much higher prior to about 3.6 Ga than since then. Extrapolation of this trend would indicate that surfaces older than ~ 4.1 or 4.2 Ga, at most, were saturated with craters, so that survival of rock of greater age would be inhibited. For actual dating of surfaces, we recommend examination of the entire size distribution of craters, not just the N(1) figure, since it measures only survival of craters at about 1 km scale. (Adapted from Neukum *et al.*, 2001).

surfaces, where the impactors are thought to come largely from the same source population. As with the Moon, geologic mapping of other planetary surfaces delineates key stages and events in the rock record that can be used to characterize and/or demarcate geologic periods. Widespread surfaces formed at or near important time boundaries can be used to determine crater size–frequency distributions, which has been done for Mars (Figure 15.2). Venus has only ~1000 craters, and, as on the Earth, this number is too small for meaningful detailed age determinations. Mercury has limited spacecraft data but shows ancient, heavily cratered surfaces similar to those of cratered lunar highland terrains. Outer planet satellites have variable cratering records that include outer solar system sources of bolides, which make their dating using crater-density techniques highly conjectural. Great strides have been made toward a useful planetary time scale (Figure 15.3), yet further advancements are needed to overcome non-uniform knowledge of the various planetary bodies and remaining, large uncertainties in many of the stratigraphic relationships, cratering rates, and other observations and processes that determine the accuracy and precision of planetary time scale boundaries.

15.2. TIME SCALES

15.2.1. Earth's Moon

Lunar stratigraphy arose from results of the US Geological Survey's systematic mapping program in the 1960s and early 1970s. At first the mapping was performed using telescopic photographs at 1:1 000 000 scale. An early model for the stratigraphy of part of the lunar nearside by Shoemaker and Hackman (1962) resulted in five time-stratigraphic systems (pre-Imbrian, Imbrian, Procellarian, Eratosthenian, and Copernican), based on mapping and superposition relations among map units of the Copernicus region, where the Copernicus and Eratosthenes craters and basin and mare-fill materials of the Imbrium impact dominate (Figure 15.4). The Lunar Orbiter IV mission of

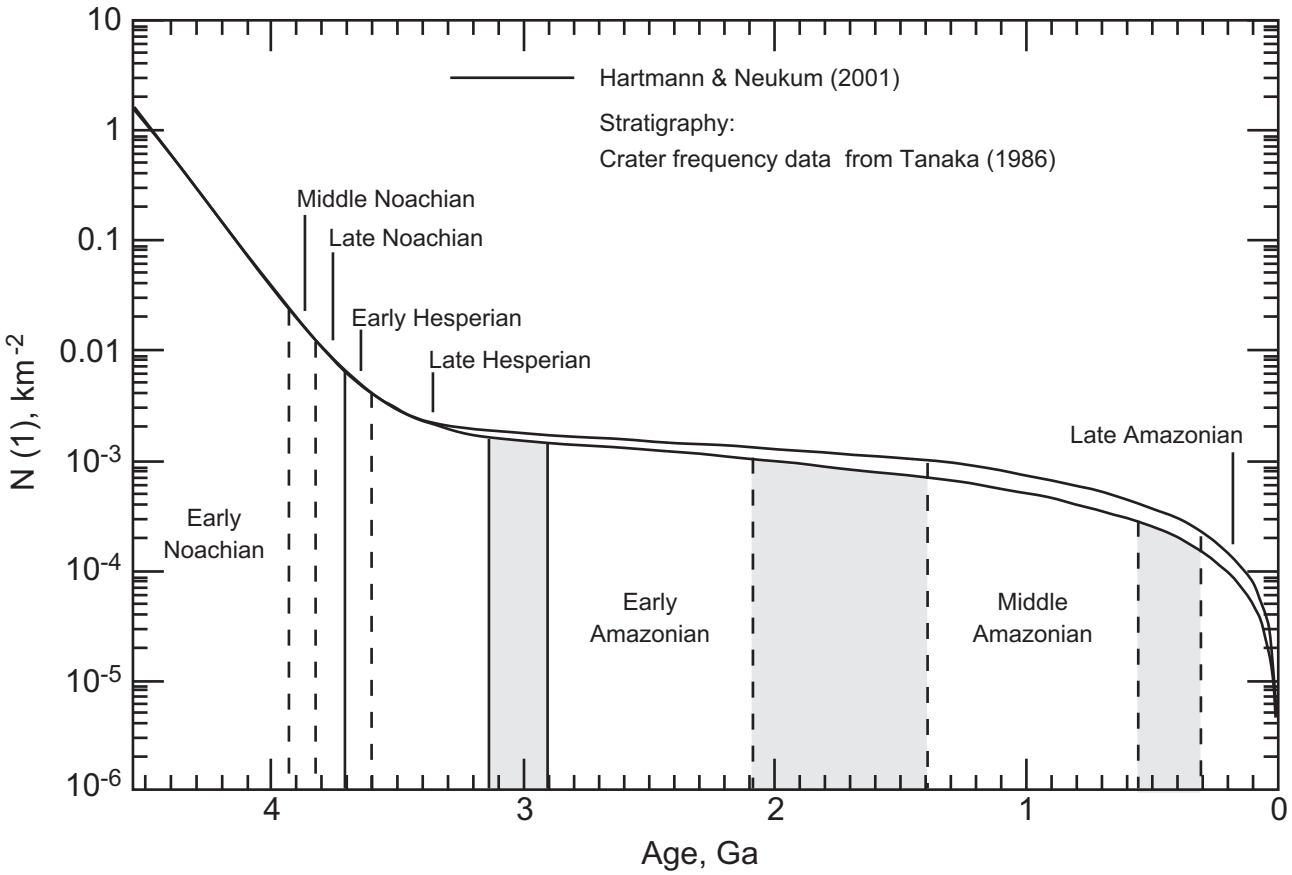

FIGURE 15.2 **Crater density vs. age for Mars.** This plot is made with a log scale in crater density. Crater density is expressed in terms of N(1) = number of craters of D >1 km, per square km. The two curves represent independent solutions by Hartmann and by Neukum. The Martian eras were defined by Tanaka entirely by crater densities. The vertical lines and shaded bands give best corresponding estimates for the divisions between the eras, based on the uncertainties in the Hartmann/Neukum curves, caused principally by uncertainty in the Martian crater production rate. For actual dating of surfaces, we recommend examination of the entire size distribution of craters, not just the N(1) figure, since it measures only survival of craters at about 1 km scale. (Adapted from Hartmann and Neukum, 2001).

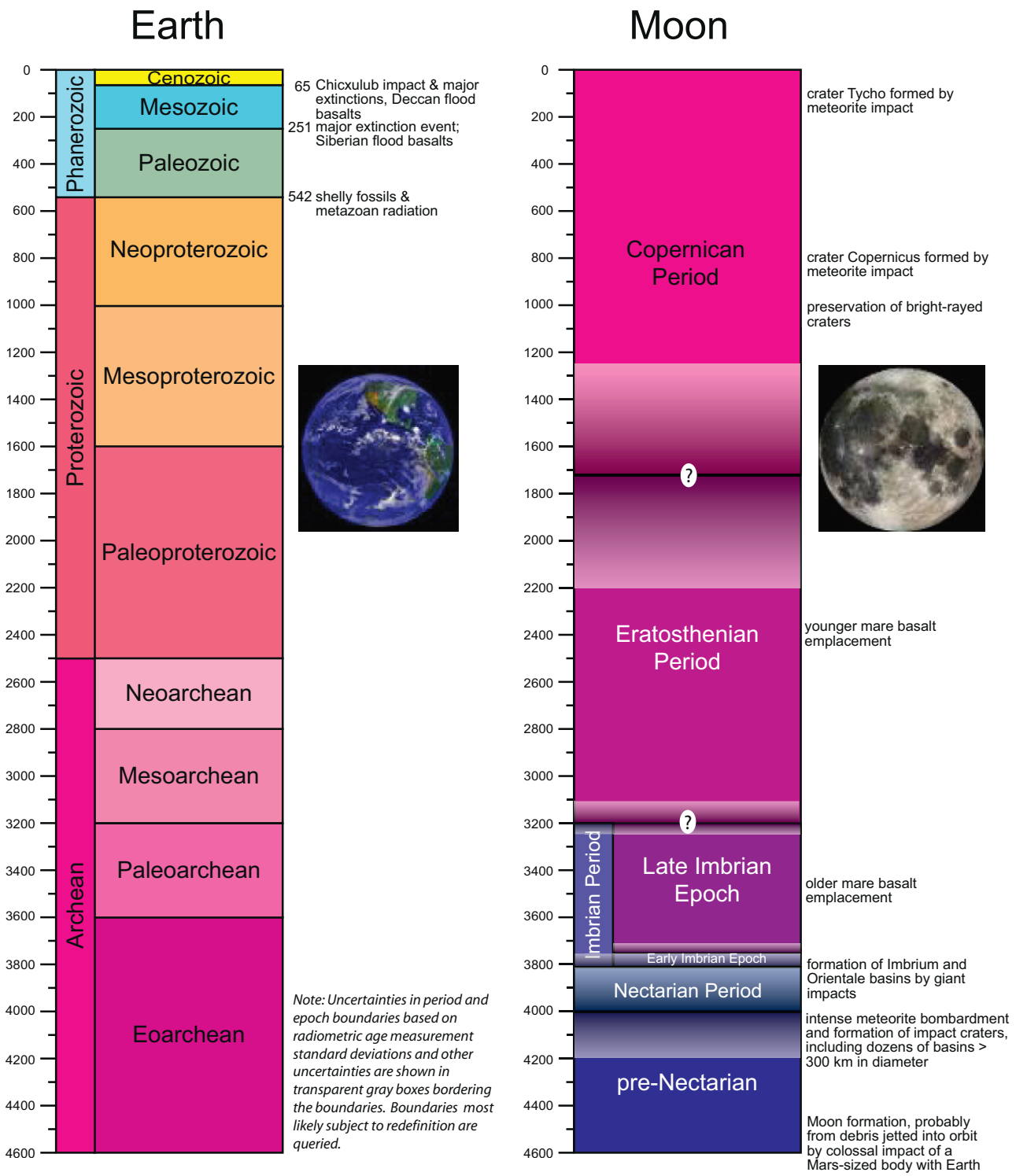

FIGURE 15.3 **Planetary time scale.** Thick dashed line separates the Venus and Mercury time scales.

1967 provided low-sun photographs of the lunar nearside at 70 to 150 m resolution – about ten times better resolution than telescopic photos (e.g., Figure 15.4). These data were used in subsequent detailed geologic maps that were published during the 1970s. Based largely on earlier mapping, a synoptic geologic map of the nearside of the Moon at 1:5 000 000 scale was published utilizing the Shoemaker and Hackman system that was tied to major impact basin- and crater-forming events (Wilhelms and McCauley, 1971). This early stratigraphy evolved over the following decades

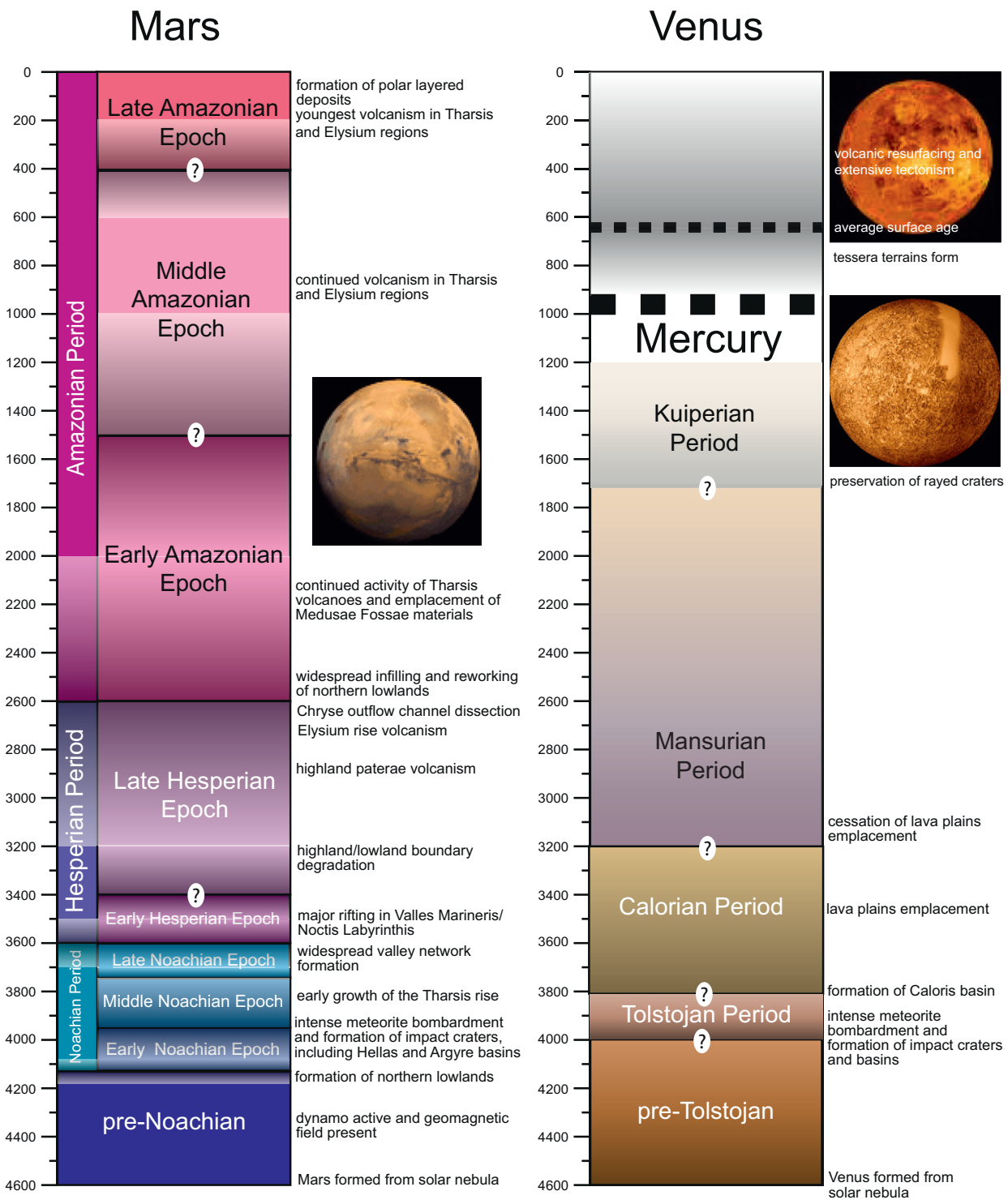

FIGURE 15.3 (*Continued*).

as further geologic mapping, crater counting, and radiometric-age analysis of returned lunar samples ensued. The most recent and significant modifications were the subdivision of the pre-Imbrian into the pre-Nectarian and Nectarian (Stuart-Alexander and Wilhelms, 1975) and division of the Imbrian System (which had earlier incorporated the Procellarian) into Upper and Lower Imbrian Series (Wilhelms, 1987) (Figure 15.5).

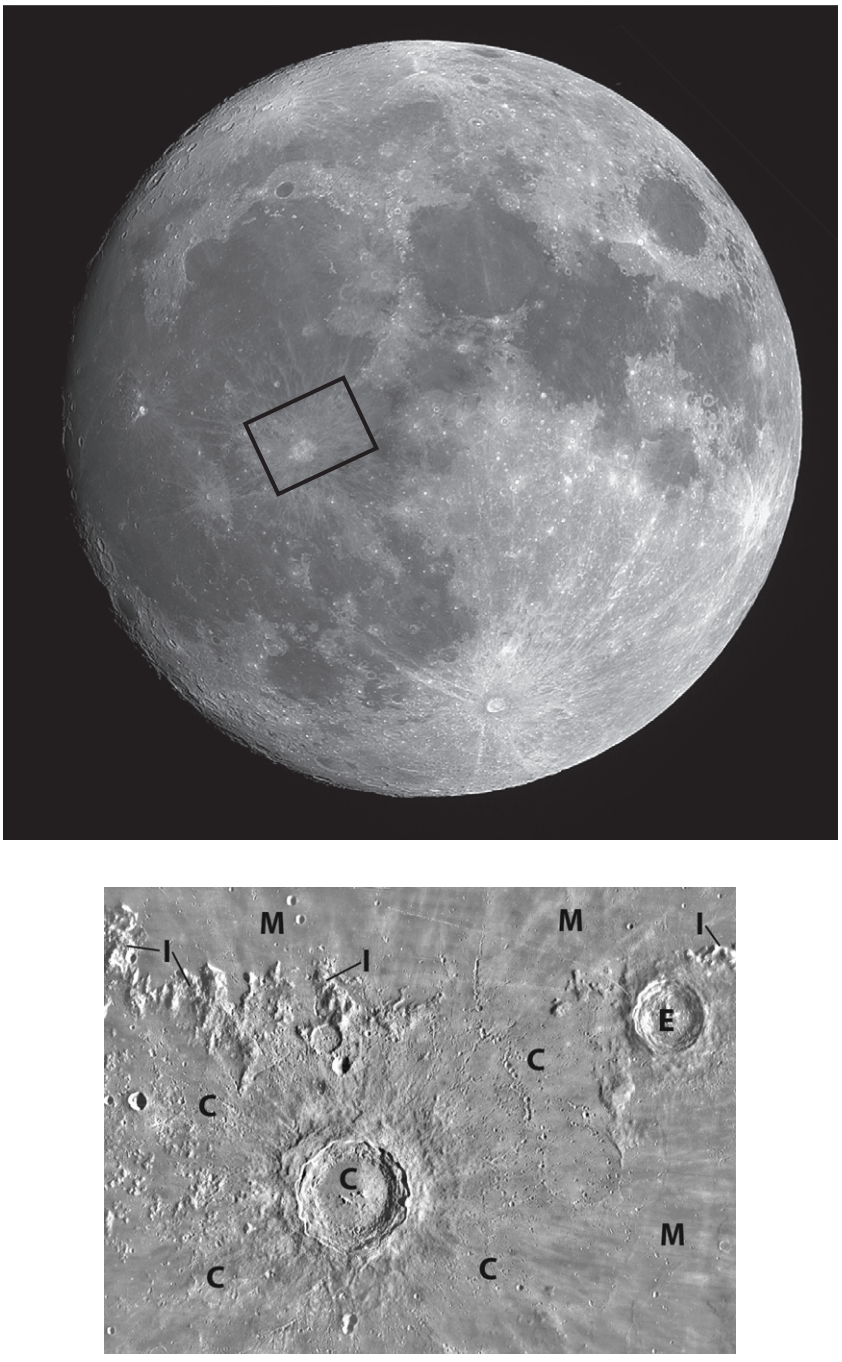

FIGURE 15.4 **A. Lunar stratigraphy: Copernicus region of the Moon.** Approximate location of this region is shown on a photograph of the Moon provided by Gregory Terrance (Finger Lakes Instrumentation, Lima, New York; www.fli-cam.com). B. Copernicus crater (C) is 93 km in diameter and centered at lat 9.7°N, long 20.1°W. Copernicus is representative of bright-rayed crater material formed during the lunar Copernican Period. Its ejecta and secondary craters overlie Eratosthenes crater (E), which is characteristic of relatively dark crater material of the Eratosthenian Period. In turn, Eratosthenes crater overlies relatively smooth mare materials (M) of the Late Imbrian Epoch. The oldest geologic unit in the scene is the rugged rim ejecta of Imbrium basin (I), which defines the base of the Early Imbrian Epoch (Lunar Orbiter IV image mosaic; north at top; illumination from right; courtesy of USGS Astrogeology Team).

In addition to superposition relations, the relative ages of lunar chronologic boundaries have been determined by impact-crater dating methods, which are based on the integrated production of craters onto a given surface from the impact of bolides (e.g., Basaltic Volcanism Study Project, 1981; Wilhelms, 1987).

The most widely used is the size–frequency method, in which crater rim diameters are measured and the

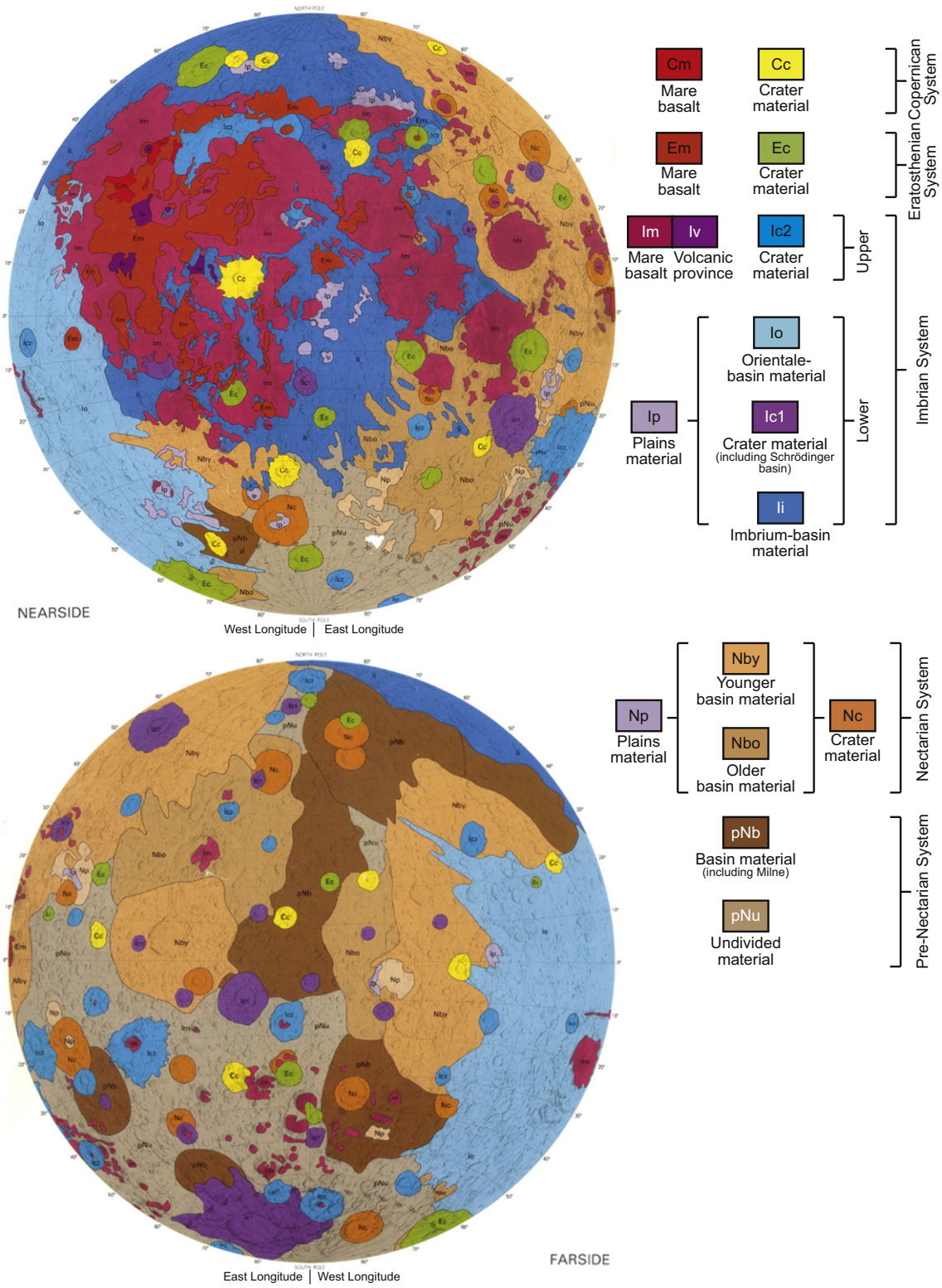

FIGURE 15.5 **Generalized geologic map of Earth's Moon.**

size−frequency distribution is plotted as number of craters per unit area vs. crater diameter on log-log plots, using either (a) cumulative densities of craters from largest to smallest, (b) incremental densities of craters in diameter bins, usually in factor of $\sqrt{2}$ increments, or (c) relative densities, in which incremental counts are normalized to a power-law function having a −3 slope (Crater Analysis Techniques Working Group, 1979). Another method that has proved useful for dating lunar surfaces is the determination of the largest craters almost destroyed on a surface by subsequent cratering erosion (Soderblom and Lebofsky, 1972; Boyce and Dial, 1975; Wilhelms, 1980).

Dozens of absolute ages have been determined by laboratory analysis of radioisotope abundances for lunar rocks using a variety of radio-isotopic-decay systems. These dates, along with inferences of their source rocks, have provided important constraints to lunar chronology (e.g., Wilhelms, 1987; Neukum and Ivanov, 1994; Stöffler and Ryder, 2001). Furthermore, crater dating methods can be calibrated statistically to radiometric dates, thus enabling determination of model absolute ages for surfaces where reliable crater density distributions can be determined (e.g., Hartmann, 1970, 1972; Ryder *et* al., 1991; Neukum *et* al., 2001).

15.2.1.1. Pre-Nectarian Period

This period covers the time from the formation of the Moon until the formation of the Nectaris impact basin, as defined by Stuart-Alexander and Wilhelms (1975). Materials of this age form the oldest lunar deposits. Exposures occur where those materials have not been subsequently buried and reworked and are concentrated in the southern latitudes, especially within the lunar farside 2500-km-diameter South Pole-Aitken basin and two nearby swaths of highland terrain that extend beyond the equator (Wilhelms, 1987). Mapped geologic units of this age include basin interior and exterior materials and intercrater terrain composed of crater and basin deposits. These materials are largely of impact origin, including ejecta forming mountainous ring structures and impact-melt deposits within basin interiors. Materials of this age are all believed to have been reworked by impacts. No surface investigation of pre-Nectarian materials has been performed yet, although they occur as fragments in samples returned from other terrains, permitting their petrologic analysis and radiometric dating. This results in large uncertainties for determinations of impact and volcanic activity during this early time, and cratering rates cannot yet be established when they were most intense, following formation of the Moon.

Rocks of this age form the early crust of the Moon, which has a low density (~3.0 g/cm^2) (Haines and Metzger, 1980) and consists mainly of the plutonic rocks anorthosite, norite, and troctolite, dubbed the "ANT" suite (Taylor, 1975; Prinz and Keil, 1977). Another important suite of rocks of the ancient lunar highlands are highly differentiated materials characterized by their enriched proportions of potassium (K), rare-earth elements (REE), phosphorus (P), and other trace elements, leading to the acronym "KREEP" (Hubbard *et al*., 1971). The textures of these rocks and their contamination by trace elements indicative of meteorite contamination suggest that they originated as impact melts (e.g., McKay *et al*., 1979). Impact melting and mixing of the early crustal rocks thus account for the rich diversity in pre-Nectarian rock composition and texture. In addition, the early crust and upper mantle are commonly believed to result from differentiation of a "magma ocean", in which the lower density ANT material buoyantly rose and separated from denser, ultramafic material (Walker *et al*., 1975). KREEP-rich rocks may result from mixing of such primitive magmas with later basaltic magma (e.g., Taylor, 1982). Thus far, pre-Nectarian volcanic rocks have not been identified with certainty and may have been extensively altered by later impacts.

Pre-Nectarian samples and fragments have been radiometrically dated from ~4.52 to 3.93 Ga using ^{40}Ar-^{39}Ar, Rb-Sr, Sm-Nd, U-Pb, and Pb-Pb methods (same methods used for younger lunar samples; see summaries in Wilhelms, 1987 and Stöffler and Ryder, 2001). Solidification of the crust was likely complex, with local hotspots, intrusions, and intense bombardment, and apparently occurred from 4.4 to 4.2 Ga, after which the 30 preserved (11 are provisional) impact basins of the period were formed. These impact basins are >300 km in diameter, the largest of which is the proposed Procellarum basin (3200 km in diameter) on the nearside, and have been divided into nine age groups based on superposition relations (Wilhelms, 1987).

15.2.1.2. Nectarian Period

The Nectarian Period began with the formation of the 860-km-diameter Nectaris basin and ended with the Imbrian impact (Stuart-Alexander and Wilhelms, 1975). Nectarian materials make up portions of the lunar highlands, originating with Nectaris and several other basin-forming impacts as well as with many scattered craters formed during this period. These materials also include local plains-forming deposits, some of which may be volcanic. Inferences from geological mapping indicate that Nectarian surfaces could have originally covered ~75% of the lunar surface (Wilhelms, 1987). Basin interior and exterior units have been divided into younger and older groups (Wilhelms, 1987). Samples were collected of materials thought to be related to three Nectarian basins − Nectaris, Serenitatis, and Crisium − by the Apollo 16, 17, and Luna 20 missions, respectively, but the relationships are inconclusive.

Nectarian materials largely consist of pre-Nectarian materials reworked by pre-Nectarian impacts prior to emplacement as Nectarian deposits. There appear to be 10 to 12 Nectarian basins >300 km in diameter, of which Crisium, at 1060 km in diameter, is the largest. The amount of Nectarian volcanism is unknown and could have been abundant

if generated by large amounts of primordial heating induced by intense bombardment; however, if most lunar volcanism resulted from radioactivity, then Nectarian volcanism may have been relatively minor. A potential line of evidence for early volcanism are the oldest mare materials that were subsequently buried by ejecta (e.g., Schultz and Spudis, 1979; Antonenko *et al*., 1995). Hawke and Bell (1981) pointed out dark halo craters, where impacts penetrated bright highland material and ejected buried dark material with basaltic spectra.

The Nectaris impact dates the beginning of the Nectarian Period. Materials possibly associated with the impact have radiometric ages of 3.92 ± 0.03 (Deutsch and Stöffler, 1987) and 3.85 ± 0.05 (Stöffler *et al*., 1985) and a model crater-density age of 4.10 ± 0.10 (Neukum and Ivanov, 1994). A disagreement exists, however, as to how to assign ages to large basin-forming events. While most workers prefer that the younger ages of molten inclusions in samples be used, Neukum and Ivanov (1994) suggest that the younger ages reflect post basin-forming events. Moreover, Hartmann (2003) suggests that impact melts >4.0 Ga were sufficiently comminuted by later impacts such that they are rarely collected or dated by radiometric techniques. This is a significant issue, because the duration of the Nectarian Period constrains the impact rate's temporal behavior. Many have advocated that the basin-forming period was short (20 to 200 million years) and therefore records a pronounced spike in the cratering rate. Such advocates call this the "lunar cataclysm" or "late heavy bombardment" (e.g., Turner *et al*., 1973; Stöffler and Ryder, 2001; Strom *et al*., 2005). Possible mechanisms that could generate such a sudden, short bombardment include formation and migration of the outer planets (Liou and Malhotra, 1997; Levison *et al*., 2001) or changes in the orbital eccentricities of Jupiter and Saturn (Gomes *et al*., 2005; Tsiganis *et al*., 2005). Others (e.g., Hartmann, 2003) suggest that a longer period of declining cratering, with spikes associated with asteroid collisions, should not be ruled out.

15.2.1.3. Early Imbrian Epoch

The Imbrium basin is the third largest known impact basin on the Moon at 1160 km in diameter. Formation of its deposits and radial groove structures define the beginning of the Early Imbrian Epoch. This huge basin includes pronounced uplifted rings and thick primary ejecta (mapped as the Fra Mauro formation) flung hundreds of kilometers across much of the lunar nearside, but much of its interior is flooded by later mare basalts. Additional primary and secondary ejecta, forming light-colored deposits, were flung further afield. Orientale basin (930 km in diameter) is the fourth largest and best-preserved of the large lunar impact basins and displays an extensive ejecta apron that partly superposes Imbrium basin ejecta. Orientale deposits are included in this epoch. Potentially, mare basalts underlie Orientale ejecta (Wilhelms, 1987), and some of the earliest exposed mare basalts in Oceanus Procellarum and Mare Nubium likely were erupted during this period (Hiesinger *et al*., 2003). All together, Early Imbrian materials covered ~20% of the Moon by the end of the epoch (Wilhelms, 1987).

KREEP-rich Imbrium basin breccia and impact melt rocks recovered at the Apollo 14, 15, and 16 landing sites yield ages which have been used to produce either a 3.85 ± 0.02 Ga (Wilhelms, 1987; Stöffler and Ryder, 2001) or a 3.77 ± 0.02 Ga (Stöffler and Ryder, 2001) age for the Imbrium basin-forming event. Orientale has not been directly sampled yet and thus does not have radiometric ages, but it appears to be older than the mare basalts dated at 3.72 Ga (Wilhelms, 1987), as its ejecta do not superpose nearby maria.

15.2.1.4. Late Imbrian Epoch

The top of the Early Imbrian Orientale basin materials defines the base of the Late Imbrian (Wilhelms, 1987). This epoch records the largest amount of mare basalts, which form two thirds of the exposed nearside maria, or about one sixth of the entire lunar surface. No large impact basins formed during this period, but impact craters and their ejecta of this age are scattered across the surface. Because the maria are plentiful and were easily accessible to surface investigations, a wealth of returned samples from Apollo 11, 15, 16, and 17 and Luna 24, along with remotely sensed data, characterize the texture, composition, and age of these materials. Mare samples discriminate multiple basalt compositions and likely eruptions at given sites, including some pyroclastic mantle deposits. However, because of impact gardening, outcrops generally are lacking and intact rocks are buried beneath a regolith several meters thick; on the other hand, impacts excavate samples from rocks buried tens of meters or more.

Geologic mapping and crater-dating studies have investigated detailed age relations within the materials of this epoch (e.g., Wilhelms, 1987; Hiesinger *et al*., 2003). Earlier materials generally occupy higher parts of the outer Procellarum basin and other isolated spots that were more readily shielded from later volcanic resurfacing. As the Late Imbrian began immediately after the Orientale impact, the age of Orientale materials date this boundary, which was assigned to 3.8 Ga and a range of 3.85 to 3.72 by Wilhelms (1987) given the ages of the Imbrium basin (see also discussion in Stöffler and Ryder, 2001) and oldest measured Late Imbrian mare basalts at the Apollo 17 site.

15.2.1.5. Eratosthenian Period

This period was introduced into lunar stratigraphy to represent a period of scattered cratering that produced deposits of low to medium albedo superposed on Imbrian materials based on telescopic observations of the Copernicus region, of which Eratosthenes crater is representative (Shoemaker and Hackman, 1962). More in-depth geological mapping and crater counting, including the use of Lunar Orbiter IV images, have indicated extensive, scattered outcrops of mare basalts

of Eratosthenian age covering about 5% of the lunar surface (e.g., Wilhelms and McCauley, 1971; Wilhelms, 1987; Hiesinger *et al*., 2003).

Stratigraphically and chronologically, the beginning of the Eratosthenian Period remains ill-defined, since dating of the Eratosthenes cratering event is not well constrained. Wilhelms (1980) correlated Eratosthenes with a sequence of mare units, and later, Stöffler and Ryder (2001) constrained the base of the Eratosthenian to at least the age of mare materials of the Apollo 12 landing site (3.15 ± 0.04 Ga) but younger than the Apollo 15 (3.30 ± 0.02 Ga) and Luna 24 (3.22 ± 0.02 Ga) mare basalts. Also to be considered is whether that event merits a global stratigraphic boundary. While there is no basin-forming impact around this time, it does appear that mare volcanism transitioned from a period of high, peak flux in the Late Imbrian to lessened and sporadic production rates at ~3.3 Ga (Hiesinger *et al*., 2003). Such a decline has a more widespread significance to lunar geologic evolution and future work might consider this as an alternative definition for the base of this period.

15.2.1.6. Copernican Period

Copernicus crater is one of the most pronounced bright-rayed craters on the lunar nearside. Shoemaker and Hackman (1962) associated the Copernican Period — the youngest era of the Moon — with the span of preserved bright-rayed craters. Since impact cratering and mare resurfacing have gradually waned, materials of the Copernican cover only a few percent of the lunar surface. Copernicus is generally dated at 800 ± 15 Ma based on the age of degassing of a granite fragment inferred to result from the Copernicus impact (Bogard *et al*., 1994), but older ages have also been proposed (see Stöffler and Ryder (2001) and references therein). However, the Copernicus crater event did not occur at or near the beginning of the record of bright-ray craters. Thus, the beginning of the Copernican remains ill-defined. Wilhelms (1987) cited the age of a sample from the Apollo 15 landing site, dated at 1.29 ± 0.04 Ga (Bernatowicz *et al*., 1978) as the oldest possible Copernican sample, which could have come from Aristillus or Autolycus craters. Ryder *et al*. (1991), however, suggested that a $\sim 2.1 \pm 0.1$ Ga date for shock-melted KREEP basalt also collected at the Apollo 15 site may be Autolycus ejecta. The relatively degraded appearance of Autolycus suggests that it may be among the oldest bright-rayed craters, and thus a candidate event for defining the beginning of the Copernican (Wilhems, 1987; Stöffler and Ryder, 2001). Although mare volcanism has been at its lowest rate during the Copernican, more than a dozen local mare surfaces have model crater ages that could be of this period (Hiesinger *et al*., 2003). The age of the youngest lunar mare volcanism remains uncertain.

15.2.2. Mars

Little detail of the surface of Mars can be resolved telescopically from Earth; thus study of its surface chronology had to await spacecraft exploration, which began in the 1960s with the Mariner missions. The stratigraphic basis for Mars was largely initiated from the US Geological Survey's program for systematic mapping of 30 quadrangles of the surface at 1:5 000 000 scale primarily using the Mariner 9 mission visible-wavelength images of the planet, mostly at 1 to 2 km/pixel resolution. This work was collated into a global map at 1:25 000 000 scale that defined the Noachian, Hesperian, and Amazonian Periods based on referent geologic terrains (Scott and Carr, 1978). The same data were used to date surfaces based on crater density determinations, and a much wider range of ages was found than on the Moon (e.g., Hartmann, 1973). Mars was revisited during the late 1970s by the two Viking Orbiters that produced tens of thousands of images

TABLE 15.1 Stratigraphic, Radiometric-Age, and Crater-Density Data for Lunar Chronologic Units

Chronologic Unit	Referent Unit	Lower Radiometric-Age Boundary (Ga)	No. Craters $\geq$ 1 km per 10^6 km^2	No. Craters $\geq$ 20 km per 10^6 km^2
Copernican Period	Bright-rayed craters (e.g., Copernicus)	2.2 to 1.25	<750 (mare) <1000 (crater)	n/a
Eratosthenes Period	Low-albedo craters (e.g., Eratosthenes)	3.24 to 3.11	750 to ~2500 (mare)	n/a
Late Imbrian Epoch	Post-Orientale mare basalts	3.80 to 3.72	~2500 (mare) to ~22 000	28
Early Imbrian Epoch	Imbrian basin materials	3.87 to 3.75	~22 000 to 48 000 (basin)	18 to 33
Nectarian Period	Nectaris basin materials	4.20 to 3.80	n/a	23 to 88
pre-Nectarian Period	n/a	~4.5	n/a	>70

See text for discussion of referent units and radiometric-age boundaries. Crater-density ranges from Wilhelms (1987: table 7.3).

covering most of the surface at 100 to 300 m/pixel or better. This resulted in an updated geological map of Mars at 1:15 000 000 scale (Scott *et al*., 1986–87) that was used by Tanaka (1986) as a basis to subdivide the three chronologic periods into eight epochs (Early, Middle, and Late Noachian; Early and Late Hesperian; and Early, Middle, and Late Amazonian) at multiple crater diameters (Figures 15.2, 15.3, and 15.6). Subsequently, the referent map unit for the base of the Amazonian Period was redefined for the surface of a widespread deposit covering much of the northern plains of Mars (Tanaka *et al*., 2005; Figure 15.7); the unit's crater size-frequency distribution is statistically consistent with the base of the Amazonian as defined by Tanaka (1986). Detailed reassessment of the crater density of this regional unit by Werner *et al*. (2011) led to a reassignment of the density of 1 km craters for this boundary by Werner and Tanaka (2011). The latter paper additionally fitted the epoch boundaries to idealized size–frequency distributions at single crater diameters and calculated ages based on the crater production models of Ivanov (2001) and Hartmann (2005). Also, an informal pre-Noachian period was defined from geologic mapping and cratering analysis largely based on a topographic model of the Martian surface derived from laser altimetry measurements from the Mars Global Surveyor spacecraft at 460 m/pixel (e.g., Smith *et al*., 1999; Tanaka *et al*., 2005; Frey, 2006). The earlier Martian epochs are commonly thought to correspond roughly with the early lunar periods, as the high impact rates and crater size–frequency distributions were shared (e.g., Neukum and Wise, 1976; Tanaka, 1986; Hartmann and Neukum, 2001; Strom *et al*., 2005).

The periods and epochs represent a collation of a complex resurfacing history involving a variety of widespread events and activities occurring over Martian geologic time. Beginning in the late 1990s, exploration of the surface of Mars has been unprecedented, involving the return of extensive imaging, topographic, spectral, and geophysical data sets from the Mars Global Surveyor, Mars Odyssey, Mars Express, and Mars Reconnaissance Orbiter spacecraft in polar orbits around the planet as well as from the robotic surface investigations of Mars Pathfinder and Mars Exploration Rovers. Observations of populations of Mars-crossing asteroids and comets and theory on their evolution provide avenues for estimating the cratering rate history of Mars, particularly when calibrated and scaled to the lunar cratering rate (e.g., Basaltic Volcanism Study Project, 1981; Neukum and Ivanov, 1994; Hartmann and Neukum, 2001; Ivanov, 2001; Neukum *et al*., 2001).

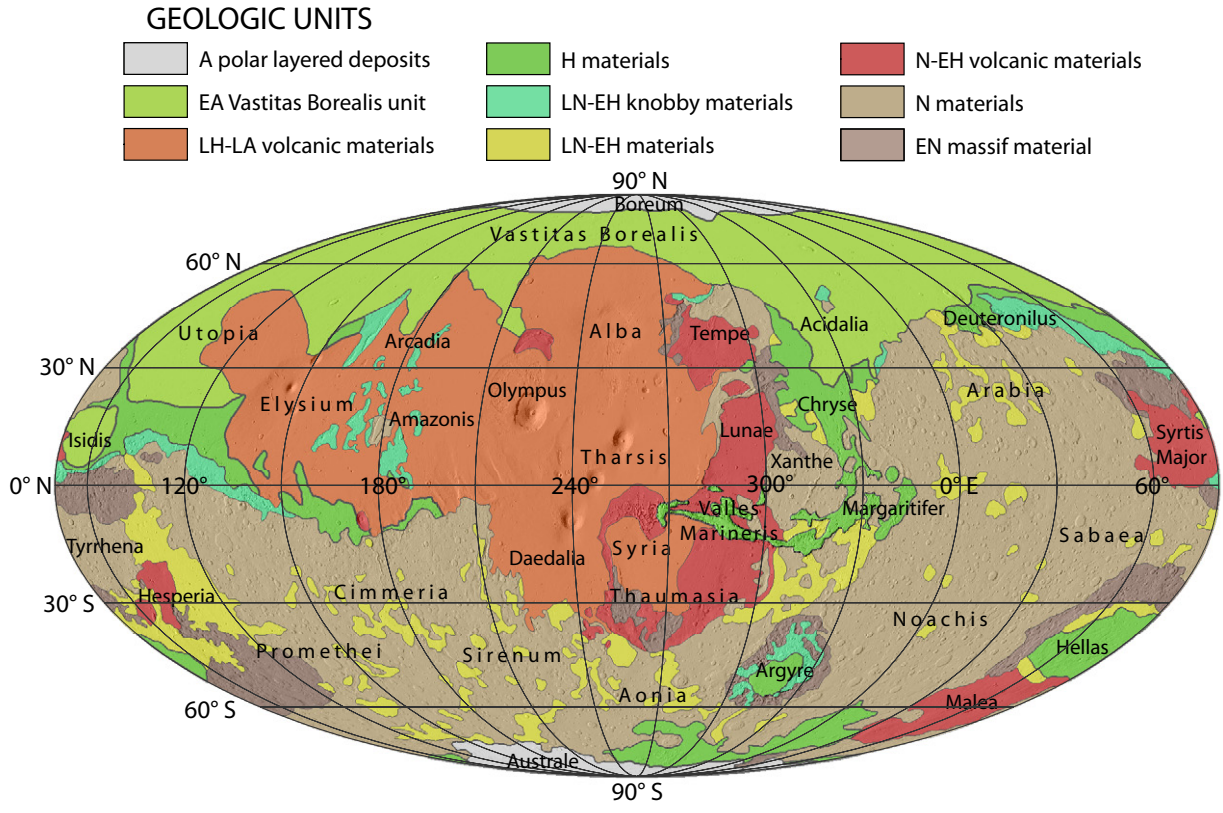

FIGURE 15.6 **Generalized geologic map of Mars showing distribution of major material types and their ages**. Chronologic unit abbreviations: N, Noachian; H, Hesperian; A, Amazonian; E, Early; L, Late. Adapted from Nimmo and Tanaka (2005). Terrain names shown without descriptor terms. Mollweide projection, using east longitudes, centered on 260°E, Mars Orbiter Laser Altimeter (MOLA) shaded-relief base illuminated from the east. On Mars, 1° latitude = 59 km.

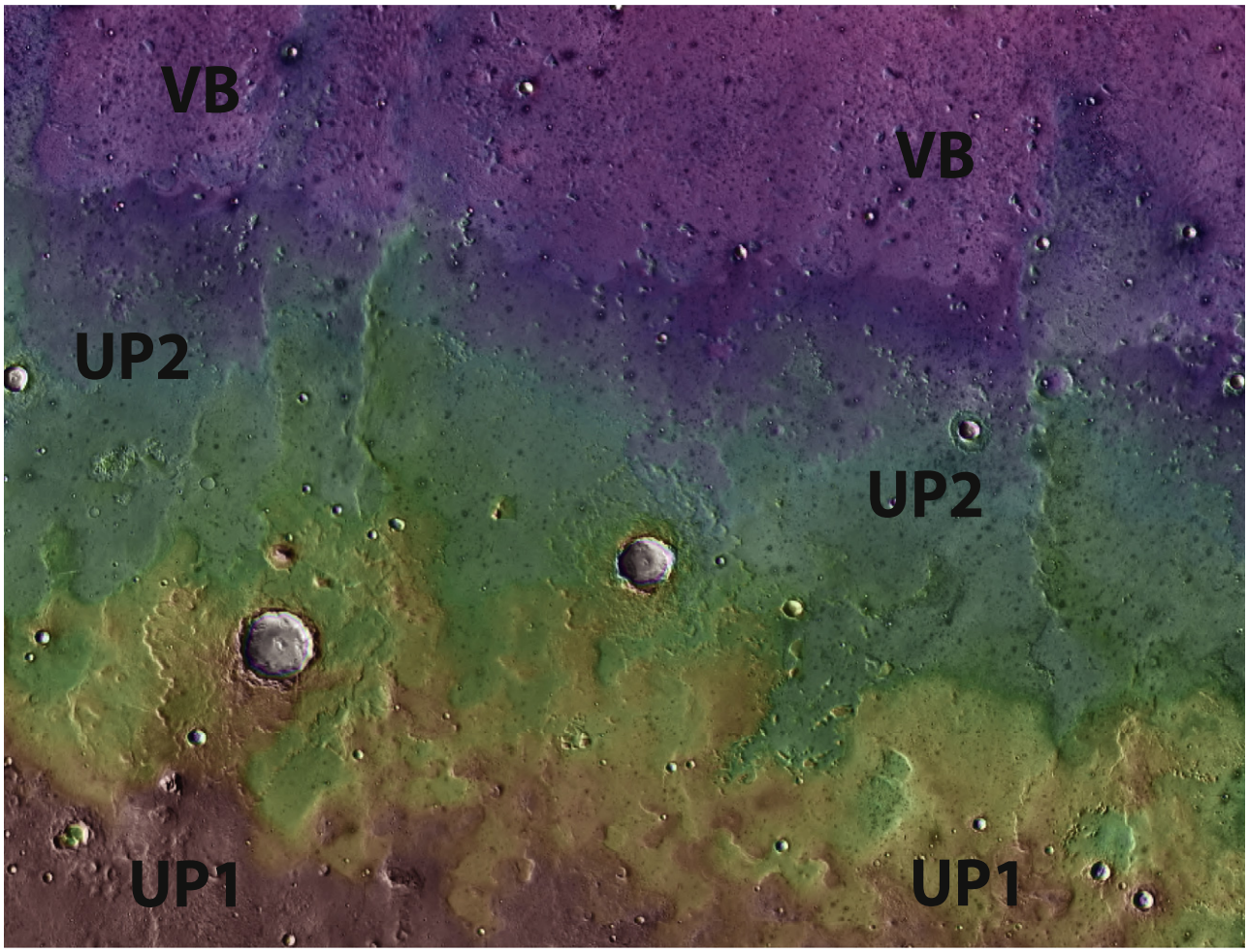

FIGURE 15.7 **Part of south-central Utopia Planitia in the northern lowlands of Mars showing geologic units from Tanaka *et al.* (2005).** Vastitas Borealis units (VB) display a relatively bright (i.e. warmer), finely ridged, and hummocky surface bordered by a lobate margin. These units define the base of the Amazonian Period. They overlie the smooth, locally knobby and ridged Late Hesperian Utopia Planitia 2 unit (UP2) that in turn embays depressions and scarps marking the rolling and hollowed surface of the Early Hesperian Utopia Planitia 1 unit (UP1). Image base (centered near 19°N, 113°E; 412 km scene width; north at top; illumination from lower left) consists of (1) a partly transparent Thermal Emission Imaging System daytime infrared image mosaic (~230 m/pixel) in which brightness indicates surface temperature, overlying (2) a color shaded-relief digital elevation model from Mars Orbiter Laser Altimeter data (brown is high, purple is low; ~460 m/pixel).

Application of the technique becomes more problematic at smaller diameters, because the initial "input" size distribution of small craters is harder to measure at small sizes. Secondary cratering and atmospheric and resurfacing effects affect small-sized craters preferentially (Chapman *et al.*, 1969; Hartmann, 1971; Chapman, 1974; Soderblom *et al.*, 1974; Basaltic Volcanism Study Project, 1981; Tanaka, 1986). Once the "input" size distribution, or "production function", has been identified, however, the losses of small craters become the very tool by which the resurfacing history can be established (Basaltic Volcanism Study Project, 1981). Such an input production function, down to decameter crater sizes, has been reportedly measured on the Moon and in numerous younger areas of Mars (Neukum *et al.*, 2001; Hartmann, 2005; Werner, 2006; Hartmann *et al.*, 2007). As an example, if a region is found where this size distribution is fitted down to diameters of 50 m, with a strong deficiency below that, it implies that erosion or deposition has obliterated craters smaller than that – meaning that the vertical extent of the erosion or deposition is of the order of the depth and/or rim height of 50 m craters. A reported detection of decameter-scale craters forming on Mars today (Malin *et al.*, 2006) suggests that in coming years it will be possible to refine our knowledge of the precise production rate and size distribution of small craters, at least in contemporary geologic time.

Considerable confusion has been introduced into this subject by recent discussions of secondary cratering. McEwen *et al.* (2005) and several other authors stated or implied that crater counts generally attempt to tabulate only primary craters, and therefore if a sizeable fraction of decameter craters are secondaries, the whole method fails. McEwen *et al.* (2005) suggest that craters <600 m in

diameter in Hesperian regions are 50% secondaries, which may be correct. These authors, however, suggested enormous errors in the crater-count methods and dates, by factors of hundreds or a thousand. Their original statement is incorrect, however, because most crater-count programs are not necessarily restricted to primaries. Hartmann (1967) noted that the discussions of decameter-scale and hectometer-scale lunar craters seen in Ranger photos raised doubts about separating primaries from secondaries, and therefore proposed that the best method for dating would be to count the total mix of semi-randomly scattered "field craters" (i.e. primaries + *scattered* secondaries), avoiding obvious clusters, rays, and other such suspected *concentrations* of secondaries. Neukum's technique counts essentially these same craters, although Neukum has estimated that most of the craters are primaries (a conclusion that may be controversial but still leads to counting all the scattered "field craters"). Thus Hartmann and Neukum and their coworkers independently count essentially the same craters. The reported formation rate of new decameter craters on Mars turned out to be much higher than predicted for primaries by McEwen *et al*. but within a factor of three of the rates used in the Hartmann and Neukum isochrons.

Additional information on the chronology and evolution of Mars is provided by meteorites found on Earth that have compositions indicating that they are rocks ejected by Martian impacts. Most of these are igneous or surface lava rocks, and they are believed to be ejected most efficiently from exposures of coherent rock such as lava plains (Melosh, 1989). Clustered ages and compositions suggest about four to nine ejection sites (Nyquist *et al*. 2001). A support for the Martian crater count dating technique is that counts in the 1970s, beginning with Mariner 9 data and prior to recognition of Martian meteorites, suggested ages of roughly to 2.0 to 0.1 Ga for typical Martian lava plains. That age range matches the age range for all but one of the Martian meteorite launch sites (the remaining site, for meteorite ALH84001, appears to have been an exposure of igneous cumulate of the ancient Martian crust).

The majority of the Martian meteorites belong to the SNC (Shergotty-Nakhla-Chassigny) classes having basalt, lherzolite, clinopyroxenite, and dunite compositions (e.g., Nyquist *et al*., 2001 and references therein). Ferric oxide-rich dust obscures detection of bedrock compositions using spectral mapping techniques for large regions of Mars; where observable, the bedrock generally has pyroxene-rich basaltic to andesitic compositions, with local areas showing concentrations of hematite, phyllosilicate minerals, and hydrated sulfates (e.g., Christensen *et al*., 2000a,b; Bibring *et al*., 2005).

As can be seen, the literature addressing the chronology of Mars is now extensive and complex, and expected new data will permit further substantive reassessments of the stratigraphic basis and crater-age modeling used in construction of the Martian time scale.

15.2.2.1. Pre-Noachian Period

This informal period covers the time between formation of the crust and development of the northern lowlands of Mars (Frey, 2005, 2006; Nimmo and Tanaka, 2005). The signature for this period is the record of "quasi-circular depressions" (QCDs) evident in the topography and interpreted to be buried impact basins (Frey *et al*., 2002). Materials of this period are not known to be preserved as exposed surface units, but it is possible that kilometers of uplift and erosion at Valles Marineris and elsewhere have exposed pre-Noachian wall rocks. In addition, fragments dating from this time are expected to be common within reworked Noachian materials. However, one such fragment may be the Martian meteorite ALH84001, which is an orthopyroxenite not of the SNC suite. ALH84001 has a range of radiometric ages between ~4.56 and 3.89 Ga; Nyquist *et al*. (2001) suggest a preferred age of 4.51 ± 0.11 Ga based on Sm-Nd isotopic abundances. Later heating, perhaps by impacts, may be responsible for the younger age derived from ^{39}Ar-^{40}Ar and Rb-Sr measurements.

Because of bombardment, not much is known about other geological activity during the pre-Noachian. Like the lunar crust, the crust of Mars may have formed by solidification of a magma ocean at ~4.5 Ga having the equivalent of a basaltic andesite or andesite composition (Nimmo and Tanaka, 2005). One apparent signature of this period is the intense crustal remanent magnetization of highland region rocks as measured by the magnetometer on board Mars Global Surveyor (Connerney *et al*., 2001). The magnetization is much weaker in and around Hellas and Argyre basins, the northern lowlands, and the Tharsis topographic rise. Formation of these features as huge impact and/or magmatic events likely obliterated the magnetic signatures, but the timing of the end of the magnetic field is uncertain. If plate tectonism was active during this period in the northern lowlands (Connerney *et al*., 1999; Fairén *et al*., 2002), it must have continued after cessation of the dynamo to account for the weak magnetic remanence in the northern lowlands. Based on the record of QCDs, pre-Noachian events by definition are not preserved in the lowland crust, but do include many of the large, basin-forming impacts that form highland QCDs (Frey, 2006). The densities of QCDs in the northern lowlands on top of Utopia and other apparent, buried basins indicate that the northern lowlands formed at $\sim 4.13 \pm 0.05$ Ga (Frey, 2006), based on extrapolation from 16 to 200 km diameter craters of the crater-density vs. age scheme of Tanaka (1986) using a -2 power law. Because these large basins are superposed on the stabilized northern lowlands but have little or no outcrop (Xanthe Montes may be vestiges of the Chryse basin rim), they define the top of the pre-Noachian.

15.2.2.2. Early Noachian Epoch

This epoch is defined by the outcrops of basin materials associated with the Hellas, Argyre, Isidis, and other impacts,

as well as isolated massif-forming materials in the Thaumasia highlands that appear heavily cratered and embayed by Middle Noachian and younger materials (Scott *et al*., 1986–87; Tanaka, 1986; Dohm *et al*., 2001; Frey, 2006). The boundaries of the Early Noachian are not precisely dated. The beginning of the Early Noachian postdates formation of the northern lowlands. Early Noachian materials cover only ~4% of the surface of Mars (Tanaka *et al*., 1988), apparently because continued impact bombardment during the Middle Noachian destroyed all but the highest-standing and perhaps most-resistant Early Noachian outcrops. Model crater ages for rim materials of Hellas, Argyre, and Isidis by Werner (2008) range from 3.99 to 3.83 Ga; 13 of 16 additional impact basins crater dated in that same study were in that age range or older (as much as 4.11 Ga), indicating that most Martian highland impact basins are Early Noachian.

15.2.2.3. Middle Noachian Epoch

In spite of the apparently short duration of this epoch, surfaces of this age now cover about a fourth of the planet but likely covered two thirds or more of the planet before they were later resurfaced. They form rugged cratered terrains made up primarily of impact ejecta and melt and unknown amounts of volcanic and sedimentary rocks (Scott *et al*., 1986–87; Tanaka *et al*., 1988). Most of the exposed Middle Noachian materials occur in the equatorial and southern highlands above the mean planetary radius (or zero elevation datum), but also include the vast Arabia Terra cratered materials at lower elevation. Although few Middle Noachian outcrops occur within the Tharsis volcanic province, such as in its Thaumasia highland region (Dohm *et al*., 2001), Tharsis may have been emerging by then as a sufficiently large volcanic rise to alter the gravity field and affect drainage patterns (Phillips *et al*., 2001). Some exposures within or beneath Middle Noachian outcrops show detections of phyllosilicates in near-infrared spectral data (Bibring *et al*., 2005). Commonly, erosional scarps and crater rims expose layered sequences in high-resolution (<10 m/pixel) images (Malin and Edgett, 2001). Valles Marineris canyons cut surfaces as old as Middle Noachian and expose layered sequences that may be largely lava flows and perhaps sedimentary rocks formed during the early growth of Tharsis (Witbeck *et al*., 1991; McEwen *et al*., 1999; Malin and Edgett, 2000).

The base of the Middle Noachian is not well defined, as stratigraphic and crater-density relations of cratered terrain materials that embay Early Noachian basin materials tend to be poorly preserved due to later resurfacing. Tanaka (1986) based his dating of the Middle Noachian on a χ^2 goodness-of-fit test between lunar Nectarian and Middle Noachian size-frequency distributions of craters >16 km in diameter using the lunar data of Wilhelms *et al*. (1978), which places the base of the Middle Noachian at 4.2 to 3.8 Ga using our inferred correlative lunar chronology (Table 15.1). The crater size distributions of these surfaces have different densities but similar log-normal forms, which may be in part due an early characteristic size–frequency distribution of impactors (e.g., Strom *et al*., 2005). This accommodates the ranges suggested by Hartmann and Neukum (2001; ~4.0 to 3.9 Ga), Hartmann (2005; ~4.1 to 3.8 Ga), and Werner and Tanaka (2011; 3.97 to 3.85 Ga).

15.2.2.4. Late Noachian Epoch

This epoch is characterized by deposition of intercrater plains materials interspersed among and embaying Middle Noachian cratered terrain materials. For the most part, subsequent cratering has obliterated morphologies that could have indicated their origins. In many cases, fluvial valleys enter into the outcrops, indicating that the materials are of fluvial or lacustrine origin (e.g., Irwin *et al*., 2002; Malin and Edgett, 2003). Some outcrops include mosaics of low knobs and mesas that indicate a disturbance and possible release of water, perhaps due to sill intrusions (e.g., Wilhelms and Baldwin, 1989). Late Noachian rocks of likely volcanic origin cover parts of the Tharsis rise, form highly degraded massifs south of Tharsis, and make up low edifices and furrowed plains on southern and northeastern parts of the Hellas rim (Scott and Tanaka, 1981; Tanaka, 1986; Crown *et al*., 1992; Leonard and Tanaka, 2001). Degradation of Late Noachian surfaces, including craters and their ejecta deposits, is pervasive and can be explained both by impact gardening and erosional effects from a thicker atmosphere and geothermal heating (e.g., Tanaka *et al*., 1998; Craddock and Howard, 2002; Irwin *et al*., 2005; Fassett and Head, 2008a,b). Altogether, exposed Late Noachian rocks cover ~12% of the planet.

Comparison of the shapes of the size–frequency distributions of craters for diameters >8 km indicate that combined Late Noachian and Early Hesperian crater distributions match the Imbrian distribution, which prompted Tanaka (1986) to assign the base of the Late Noachian to the age of the base of the Imbrian (3.80 to 3.72 Ga according to Table 15.1). Hartmann and Neukum (2001) indicate that the base of the Late Noachian is ~3.80 Ga and Hartmann (2005) suggests ~3.9 to 3.6 Ga (which encompasses the 3.86 to 3.85 Ga age range of Werner and Tanaka (2011)); the latter, more conservative estimate is used herein. Tanaka (1986) assigned crater density ranges to the Late Noachian (Table 15.2) based on measurements for parts (not all) of the mapped Late Noachian outcrops.

15.2.2.5. Early Hesperian Epoch

Hesperian and younger rocks generally have sufficiently well-preserved morphologies such that primary forms and textures of lava flows, small volcanoes, impact craters, and other similar features are recognizable. This appears to result from

TABLE 15.2 Referent Units and Crater-Density Data and Model Absolute Ages for Bases of Martian Chronologic Units.

Chronologic Unit (Epoch)	Referent Unit	No. Craters $\geq$ 1 km per 10^6 km^2	No. Craters $\geq$ 5 km per 10^6 km^2	No. Craters $\geq$ 16 km per 10^6 km^2	Model Age of Lower Boundary (Ga)
Late Amazonian	Cerberus plains lava flows	<160	n/a	n/a	0.6 to 0.2
Middle Amazonian	Lava flows, Amazonis Planitia	160 to 600	<25	n/a	2.1 to 1.0
Early Amazonian	Vastitas Borealis materials	600 to 2100	25 to 67	n/a	3.46 to 2.0
Late Hesperian	(Outflow-channel deposits)	2100 to 3000	67 to 125	n/a	3.65 to 3.2
Early Hesperian	Ridged plains material	3000 to 4800	125 to 200	<25	3.74 to 3.5
Late Noachian	Intercrater plains material	n/a	200 to 400	25 to 100	3.9 to 3.6
Middle Noachian	Cratered terrain material	n/a	>400	100 to 200	4.2 to 3.8
Early Noachian	Basin rim material	n/a	n/a	>200	4.18 to 4.08
pre-Noachian	n/a	n/a	n/a	n/a	~4.5

Chronologic and referent units and crater densities from Tanaka (1986) and Werner and Tanaka (2011). See text for discussion of model age boundaries and Late Hesperian referent unit.

declines in the cratering rate and in atmospherically driven resurfacing, including precipitation-fed erosion. Crater-density determinations have greater accuracy than for Noachian surfaces as superposed craters can be more reliably discriminated from partly buried ones (e.g., Scott and Tanaka, 1981). Because of the decline in fluvial erosion, it appears likely that most Early Hesperian and younger materials scattered across the highlands and stacked within the canyons of Valles Marineris are lava flows and volcanic air-fall and other aeolian deposits (Scott *et al*., 1986–87; Chapman, 2002; Chapman and Tanaka, 2002; Irwin *et al*., 2002; Hynek *et al*., 2003). Deposits covering much of the floor of Hellas basin appear to be Early Hesperian and may have aeolian and/or fluvial/lacustrine origins (Tanaka and Leonard, 1995; Moore and Wilhelms, 2001). Locally, higher plains material along the highland/lowland boundary may have been formed by mass-wasting of Noachian materials (Tanaka *et al*., 2003, 2005). Collectively, Early Hesperian materials cover ~16% of Mars.

The base of the Hesperian was originally assigned to the base of plains-forming material making up Hesperia Planum (Scott and Carr, 1978). However, this outcrop, while representative of materials of this age, does not amount to a well-constrained stratigraphic marker that can be used globally. Tanaka (1986) measured a collective crater-density range for this outcrop and for other Early Hesperian materials to define crater ranges for this epoch (Table 15.2).

15.2.2.6. Late Hesperian Epoch

The Late Hesperian is not clearly defined stratigraphically at present. Formerly, the epoch was based on materials of the northern plains (the Vastitas Borealis Formation) as mapped and characterized using Viking data (Scott *et al*., 1986–87; Tanaka, 1986). However, more recent mapping using Mars Global Surveyor and Mars Odyssey altimetry and image data reassigned the surface of those materials to the base of the Amazonian (Tanaka *et al*., 2005). This reassignment was not sufficient to require changing the ranges of crater densities for the Late Hesperian, as the Vastitas Borealis materials display fairly uniform crater densities overlapping those defining the Hesperian/Amazonian boundary (Tanaka, 1986). Given this reassignment, Late Hesperian materials cover nearly 10% of the planet. Other Late Hesperian materials include extensive lava flows and volcanoes in the Tharsis and Elysium regions, materials of outflow channels originating in Xanthe Terra and entering into Chryse Planitia, south polar Dorsa Argentea ridged plains deposits, and higher elevation plains deposits of the northern lowlands (Scott *et al*., 1986–87; Witbeck *et al*., 1991; Tanaka and Kolb, 2001; Tanaka *et al*., 2005). The lava flows of this age are more distinct in morphology than those of the Early Hesperian and may reflect a more viscous rheology and less impact gardening. Radar sounding of the Dorsa Argentea materials indicate that they are low-loss materials likely to be ice-rich, which would indicate that the

materials may have been frozen for >3 billion years (Plaut *et al*., 2007).

The base of the Late Hesperian presently lacks a definitive stratigraphic referent unit and is for now defined by the N(5) =125 crater density (Table 15.2), which is readily measured on surfaces of about this age. Correspondingly, Hartmann and Neukum (2001), Hartmann (2005), and Werner and Tanaka (2011) provide model age estimates for this boundary that range from 3.65 to 3.2 Ga.

15.2.2.7. Early Amazonian Epoch

The Amazonian Period on Mars was originally defined using Mariner 9 images as the base of a cratered plains unit in southwestern Amazonis Planitia (Scott and Carr, 1978). Revised mapping using Viking Orbiter images was the basis for reassigning the beginning of the Amazonian to the base of a smooth plains material making up the lowermost member of the Arcadia Formation in southern Acidalia Planitia (Tanaka, 1986). Contact relations have been difficult to establish with confidence because of their subtlety as expressed in the Mariner 9 and Viking Orbiter images. Those difficulties have been largely overcome with laser altimetry data and high-resolution visible-range images from Mars Global Surveyor and thermal infrared and visible-range images from Mars Odyssey. With the new data sets, the base of the Amazonian was again redefined, but finally with much more secure observations, as the surface of Vastitas Borealis units that cover much of the northern plains (Tanaka *et al*., 2005). These materials were thought to be voluminous deposits of the Xanthe Terra outflow channels (e.g., Parker *et al*., 1989; Tanaka *et al*., 2001; Kreslavsky and Head, 2002); however, more recent data show that the deposits embay the outflow channel floors and appear heavily reworked by periglacial and soft-sedimentary style processes, as are parts of higher northern plains units (e.g., Tanaka *et al*., 2003; Skinner and Tanaka, 2007). The Vastitas Borealis units and a similar unit covering the Isidis basin floor have fairly uniform densities of craters >5 km in diameter and thus appear to constitute an extensive, collective unit of relatively uniform age that covers one eighth of the planet as presently exposed. Additional Early Amazonian materials include extensive lava and sedimentary flows of the Tharsis and Elysium rise and adjacent plains and early sequences of layered, friable materials of the Medusae Fossae Formation of possible volcanic origin (Scott and Tanaka, 1982; Chapman, 2002; Hynek *et al*., 2003). Some flows of the Elysium rise bury extensive tracts of the Vastitas Borealis units in Utopia basin. Altogether, Early Amazonian materials cover about 20% of the planet.

The surface of the Vastitas Borealis units that define the beginning of the Early Amazonian possibly constitutes the longest exposed major stratigraphic contact anywhere in the solar system, and the surface of the units is perhaps the most widespread, continuous surface of relatively uniform age as well. Craters >1 km in diameter superposed on the unit are well preserved and readily discriminated from the rimless, circular depressions that apparently mark buried craters and have a cumulative N(1) density of ~1200 determined from counts at multiple sites (Werner *et al*., 2011). Because of uncertainties in Martian crater production around this time and the varied crater-density boundaries selected, model ages vary extensively, including 3.3 to 2.9 Ga (Hartmann and Neukum, 2001), 3.2 to 2.0 Ga (Hartmann, 2005), and 3.46 to 3.00 Ga (Werner and Tanaka, 2011). The modified definition for the beginning of the Amazonian would readjust the N(1) density for the boundary to ~70 to 75, which would lead to a modest, ~0.1 to 0.2 Ga increase in model age estimates. Another significant aspect of this surface is that it displays a steeper crater size–frequency distribution for craters >5 km in diameter (~−2 power-law slope) than nearly all other surfaces on the Moon and Mars in this crater diameter range. If this unique character reflects the pristine form of the crater size–frequency distribution, then it would indicate that crater counts for other surfaces generally are affected by relatively higher obliteration of smaller craters and by contamination of larger, buried craters (Tanaka *et al*., 2006).

15.2.2.8. Middle Amazonian Epoch

Two lava plains units mapped in Amazonis Planitia using Viking Orbiter images were used originally to define the beginning of the Middle Amazonian (Tanaka, 1986). This region forms an essentially flat surface at kilometer scales (Kreslavsky and Head, 2000). Some channel features on part of this surface could be either lava or water-flooding features (Fuller and Head, 2002). Post-Viking geologic mapping of the northern plains resulted in improved mapping of the plains units in this area, as the lava flow margins and their flow patterns are much better resolved in the higher quality and higher resolution data. Two lava plains units are now mapped in northern Amazonis Planitia, which span the Middle Amazonian (Tanaka *et al*., 2005). Additional materials of Middle Amazonian age include a broad apron of lava flows surrounding the Tharsis Montes and extensive tracts of the highly eroded Medusae Fossae Formation (Scott *et al*., 1986–87). The formation age of the aureoles of Olympus Mons also appears to be Middle Amazonian (Tanaka *et al*., 2005). Middle Amazonian rocks cover about 8% of the planet.

Given the relatively limited extents and complex histories of all Middle Amazonian materials, it appears that a globally meaningful referent geological unit to define the base of the Middle Amazonian is lacking. Of the two presently mapped lava plains units of northern Amazonis Planitia, the Amazonis Planitia 1 north unit is the oldest and thus the best candidate for a revised referent unit for the Middle Amazonian. Whereas detailed crater counts of this unit are presently lacking, its N(5) density of 21.1 ± 3.9 is about right according

to the crater-density boundaries of Tanaka (1986; see also Table 15.2). Model ages for the beginning of this epoch are highly uncertain because of permissible ranges in cratering rates over this part of Martian history. Recently proposed values include 2.1 and 1.4 Ga (Hartmann and Neukum, 2001), ~2.0 to 1.0 Ga (Hartmann, 2005), and 1.45 Ga to 880 Ma (Werner and Tanaka, 2011). These constraints indicate that some of the Martian meteorites may have originated from Middle Amazonian materials. The Chassigny (dunite) and Nakhlites (clinopyroxenites) have ages of ~1.35 and ~1.30 Ga, respectively, and are cumulate plutonic rocks indicative of slow cooling and gradual crystallization (e.g., Nyquist *et al*., 2001 and references therein).

15.2.2.9. Late Amazonian Epoch

Mars has remained a geologically dynamic planet through this most recent era. The Late Amazonian Epoch was defined by Tanaka (1986) using the plain of southern Elysium Planitia as the referent. This plain appeared smooth in Viking Orbiter images and small shields and fluvial channels emanating from fissure systems in the plain were recognized. Most workers now recognize the plain as volcanic; however, multiple episodes of volcanism and fluvial discharge complicate its history (e.g., Keszthelyi *et al*., 2000; Burr *et al*., 2002; Plescia, 2003; Tanaka *et al*., 2005). Late Amazonian materials also make up the youngest lava flows of the Tharsis Montes and Olympus Mons, lava flows of southeastern Amazonis Planitia, the youngest outcrops of the Medusae Fossae Formation, a mantle deposit in northwestern Utopia Planitia, ice and dust deposits of the polar plateaus, and largely frozen dunes surrounding the north polar plateau (Tanaka, 1986; Tanaka *et al*., 2005). These materials cover 4% of Mars.

Post-Viking mapping and crater-dating studies indicate that most of the original referent unit of the Late Amazonian is generally much younger and more stratigraphically complex than previously thought. This in part appears to result from the fact that the lava flows are thin, and thus only partly bury craters superposed on underlying surfaces. This was observed by Tanaka (1986), but its effect was not then fully appreciated. Tanaka *et al*. (2005) remapped the materials into two Late Amazonian units − the Cerberus Fossae 2 and 3 units − of which the younger unit covers the lower plains of Elysium Planitia and extends down Marte Vallis into southern Amazonis Planitia. The older unit, which they also designated as Late Amazonian, crops out in higher plains areas, mostly north and west of the younger unit. Detailed studies using Viking and Mars Global Surveyor images indicate local model ages on the plains and associated Marte Vallis channel system of 200 to a few Ma (Berman and Hartmann, 2002). The youngest model ages (<100 Ma) generally rely on craters smaller than 100 m in diameter. Although McEwen *et al*. (2005) suggest that populations of craters <100 m in diameter have high proportions of secondary craters for Late Amazonian surfaces, it appears that complications from secondaries may be negligible both in Elysium Planitia and on a few Middle to Late Amazonian flows of southeastern Amazonis Planitia (Amazonis Planitia 2 south unit of Tanaka *et al*. (2005)) where crater size−frequency distributions follow expected isochron shapes down to 16 m diameters (Hartmann, 2007). Note that if anomalously high concentrations of secondaries were present in these areas, the true ages would be even younger than the inferred model ages. Detailed crater counts of the Cerberus Fossae 2 unit, which may more fittingly define the base of the Late Amazonian, have not been counted in detail. Based on the crater density assignment of Tanaka (1986), the base of the Late Amazonian has model ages of 550 and 300 Ma (Hartmann and Neukum, 2001), 600 to 200 Ma (Hartmann, 2005), and 387 to 235 Ma (Werner and Tanaka, 2011). These age ranges indicate that the basaltic and ultramafic, lherzolitic Martian meteorites known as Shergotites formed during the early part of this epoch (most workers agree with crystallization ages ranging from ~500 to 150 Ma (Nyquist *et al*., 2001), although older ages have been suggested (Bouvier *et al*., 2005)). Whereas the entire suite of Martian meteorites has >100 Ma crystallization ages, dating of their ages of ejection from Mars using cosmic ray exposure dating and their residence times on Earth indicate a range from about 20 to 0.7 Ma (Nyquist *et al*., 2001 and references therein). Bombardment on Mars continues apace with predicted cratering rates, as evidenced by detections of primary craters 2 to 125 m in diameter formed over a seven-year period (Malin *et al*., 2006; Hartmann, 2007).

15.2.3. Mercury

Mercury has been labeled an "end-member planet" due to being closest to the Sun. Its extremes include: the highest density among the planets, the most intense solar radiation and tidal forces, the highest diurnal temperature range, and the most altered geochemistry from its primordial state (Chapman, 1988). Mercury is too distant and too close to the Sun to achieve effective geological data from Earth-based observations. The three flybys of Mercury by Mariner 10 in 1974 and 1975 yielded image data at 100 to 1500 m/pixel for much of one side. Because these were flybys and not orbits, the data are foreshortened at the limbs, and the lighting geometries were similar. Morphologic details are enhanced by shading near the terminator, whereas albedo is more defined near the limbs. Some stereo imaging also yields topographic information. These data were used to produce initial geological maps, and then all or parts of 9 quadrangles of a series of 15 quadrangles covering Mercury at 1:5 000 000 scale. From the geological mapping, the first proposed stratigraphy was developed around the Caloris group of map units (Schaber and McCauley, 1980; McCauley *et al*., 1981).

Spudis (1985; see review by Spudis and Guest, 1988) expanded this scheme to apply across the imaged part of the planet, based on an unpublished global geologic map by P.D. Spudis (see review by Spudis and Guest, 1988).

In general, the major geologic events across Mercury recorded by its surface morphology and albedo closely correspond with the sequence of events recorded on the surface of Earth's Moon. The informal pre-Tolstojan period occurred prior to the Tolstoj basin-forming event and includes the earliest signatures of multi-ring basins. In most of these, one ring tends to dominate in morphologic expression and is thought to constitute the actual crater rim. The basins <500 km in diameter were largely erased during emplacement of widespread intercrater plains material also during this period, which are commonly thought to be of impact and at least partly volcanic origin (Strom, 1977). The Tolstojan Period began with emplacement of a lineated terrain unit associated with the Tolstoj basin impact, named the Goya Formation. Additional Tolstojan deposits include scattered crater, basin, and smooth plains materials. The Caloris basin impact marks the beginning of the Calorian Period. This huge impact, equivalent to the Imbrium and Orientale basins of the Moon, was only partly imaged by Mariner 10. It profoundly resurfaced Mercury and provides a distinctive stratigraphic marker (e.g., Schaber and McCauley, 1980; McCauley *et al*., 1981; Guest and Greeley, 1983). Materials of the Caloris Group include units related to basin melt and rim materials and primary and secondary ejecta, including some lineated ejecta. Hilly and furrowed material occurs antipodal to Caloris basin and is thought to result from global focusing of seismic waves from the impact (e.g., Schultz and Gault, 1975). Caloris displays as many as six basin rings and appears to be extensively flooded by lavas that infilled the basin floor soon after the impact; in turn, the lavas have been deformed by wrinkle ridges and fractures (Spudis and Guest, 1988). Post-Caloris smooth plains material of possible volcanic origin also occurs extensively outside of the basin, and additional craters and small basins formed during the remainder of the Calorian Period. The Mansurian Period begins with the formation of Mansur crater and includes slightly degraded craters lacking bright rays and containing in some cases smooth crater-floor materials probably made up of impact melt. The base of the Kuiperian Period is ill-defined; this period covers formation of bright-rayed craters as represented by Kuiper crater.

Table 15.3 shows the lunar counterparts to the Mercurian periods as suggested by Spudis and Guest (1988). The geologic evolution is remarkably similar in style, and hence has similar referent units used to define the base of each formal period. The Mercurian stratigraphic scheme shares some of the same weaknesses as the lunar one, such as the poor definition of the youngest Mansurian and Kuiperian Periods. Moreover, the large crater and basin size–frequency distributions of heavily cratered terrains on the Moon and Mercury have similar forms (Strom and Neukum, 1988; Strom *et al*., 2005). The model ages are thus borrowed from the lunar scale in Table 15.1. However, the relative cratering rates between the Moon and Mercury are not well known. As discussed by Chapman (1988), a large remnant population of near-sun heliocentric planetesimals may have been relatively slowly swept up by Mercury, thereby increasing its cratering rates following late heavy bombardment in relation to the Moon. However, astronomical searches for such objects thus far have not found any (Leake *et al*., 1987). Assuming that such objects are not significant, Strom and Neukum (1988) estimated relative cratering rates between the Moon and Mercury. They proposed that Caloris basin formed at the end of heavy bombardment at ~3.85 Ga and used this as a tie point to determine other Mercurian ages. These include 4.06 Ga for

TABLE 15.3 Referent Units, Lunar Counterparts, and Crater-Density Data and Model Absolute Ages for Bases of Mercurian Chronologic Units.

Period	Referent Unit	Lunar Counterpart	No. Craters ≥ 20 km per 10^6 km^2	Lower Lunar Model Age Boundary (Ga)
Kuiperian	Bright-rayed craters (e.g., Kuiper)	Copernican	n/a	2.2 to 1.25
Mansurian	Slightly degraded craters (e.g., Mansur)	Eratosthenes	$<24 \pm 7$	3.24 to 3.11
Calorian	Caloris Group	Imbrian	58 ± 13	3.87 to 3.75
Tolstojan	Goya Formation	Nectarian	85 ± 14	4.20 to 3.80
pre-Tolstojan	n/a	pre-Nectarian	~>85	~4.5

Most data from Spudis and Guest (1988). Model age boundaries are assumed to be roughly equivalent to those of their lunar counterparts (Table 15.1). The crater-density boundary for the Mansurian is a maximum, based on the lowest crater-density measured for smooth plains material (Spudis and Guest, 1988, table III).

Tolstoj basin and 4.02 to 4.22 for intercrater plains, which are consistent with the lunar counterpart ages.

15.2.4. Venus

The surface of Venus remained obscure to human observers until powerful radars could be used to transmit microwaves through its dense atmosphere and receive echoed signals that could image topography for morphologic analysis, as well as measure altitude, roughness, reflectivity, emissivity, and other wavelength-dependent physical properties of the surface. The radars that have been used include Earth-based Arecibo and Goldstone antennae and those flown by the Pioneer Venus Orbiter, Venera 15 and 16, and Magellan orbiting spacecraft, of which the latter provided the largest amount and highest quality of data return. Additional information about the surface was recovered by the Venera, Vega, and Pioneer Venus landers, which mostly indicated basaltic compositions (e.g., Grimm and Hess, 1997).

The surface of Venus is dominated by lavas, volcanoes, and intensely deformed terrains dotted by nearly a thousand impact craters and surficial materials produced by impacts and by the debris generated by bolides that disintegrated as they entered the atmosphere. An ongoing geological mapping program of Venus, managed by the US Geological Survey and supported by NASA, began in 1993 using the Magellan data as well as many other studies and has contributed to an understanding of its stratigraphic history. Because of the paucity of superposed craters on Venusian terrains, crater-density based investigations of surface units indicate a generally young surface. The details of the stratigraphy are suggestive but not definitive. The most consistent geologic relation is that the complex and intensely deformed terrain type generally known as tessera forms the oldest exposed materials. Its crater age reflects the mean age of cessation of sufficient deformation to destroy craters. What is controversial is to what degree stratigraphic relations evident at local scales can be extrapolated to regional and global scales, where crater-counting constraints are not definitive. There are global progressions evident in the mean crater densities for tessera, types of volcanic plains, and volcano types that might support planetwide surface evolution (e.g., Namiki and Solomon, 1994; Price and Suppe, 1995; Price *et al*., 1996), possibly justifying establishment of a system of discrete chronologic units (Basilevsky and Head, 1995; Basilevsky *et al*., 1997). Alternatively, Guest and Stofan (1999) and Hansen (2000) suggested that Venusian surface evolution has been complex, with overlapping ages of formation of the various types of volcanic and tectonic features that the planet displays and that crater-density data for large groupings of features and outcrops must be used cautiously, if at all (Hamilton and Stofan, 1996; Chapman and Zimbelman, 1998; Guest and Stofan, 1999; Hansen, 2000). The spread in crater densities based on geological terrain types, however, appears to be sufficient to refute early proposals that Venus underwent a relatively brief, catastrophic resurfacing event a few hundred million years ago (Hauck *et al*., 1998). Nevertheless, the introduction of large amounts of water and sulfur dioxide into the atmosphere from intense volcanism or a large comet impact could have led to sufficient greenhouse heating to largely control the global evolution of volcanism and tectonism, by altering the mechanical properties and thermal stress state of the lithosphere (Solomon *et al*., 1999; Bullock and Grinspoon, 2001).

The mean surface age of Venus is calculated from the planetwide crater density and estimated cratering rate. Strom *et al*. (1994) indicate that this age is 288 $+311/-98$ Ma (or range of 599 to 190 Ma), Neukum and Ivanov (1994) suggest 630 ± 100 Ma, and McKinnon *et al*. (1997), given their results ($\sim 750 \pm 50$ Ma) and that of previous workers, conclude that 1000 to 300 Ma may be acceptable. These ages suggest that mantle-plume driven resurfacing on Venus has resulted in an overall resurfacing rate over the past several hundred million years that is significantly higher than those of Earth's Moon, Mars, and Mercury, where volcanism has declined over time, but less than that of Earth, where plate tectonics has dominated resurfacing.

15.2.5. Other Cratered Bodies

These include small bodies of the inner system, such as the moons of Mars, Phobos and Deimos, and the asteroids, as well as outer planet satellites of Jupiter, Saturn, Uranus, and Neptune. None of these have formal stratigraphic systems, but some have simple to complex resurfacing histories that have been investigated by geological mapping and crater-density determinations. Also of interest are the size–frequency distributions and orbits of asteroids and comets that provide the current population of objects from which impacts occur. Knowledge of these objects can be used to model current and past impact rates and crater size–frequency distributions (e.g., Zahnle *et al*., 1998, 2003; Schenk *et al*., 2004; Strom *et al*., 2005).

Images of the asteroids Gaspra, Ida, and others taken by various spacecraft and the Martian moons Phobos and Deimos taken by Mars orbiters, show that these primordial objects have lunar-like crater size–frequency distributions, including densities indicative of equilibrium saturation in smaller diameter ranges (e.g., Neukum and Ivanov, 1994; Chapman *et al*., 1996; Veverka *et al*., 1997). However, the asteroid Itokawa observed by the Hayabusa spacecraft is an uncratered (yet impacted) rubble pile thought to have been produced by re-agglomeration and sporadic impact shaking of a broken-up parent asteroid (Fujiwara *et al*., 2006), which may be a common make-up of larger asteroids (Whiteley *et al*., 2002). Telescopic observations of main-belt asteroids (e.g., Jedicke and Metcalfe, 1998; Yoshida and Nakamura, 2004) verify that

largely the same population of projectiles, mainly asteroids, has dominated the crater population of the inner solar system (Neukum *et al*., 2001). However, asteroid bombardment rates on planetary surfaces may include significant spikes caused by the breakup of asteroids that shower asteroid fragments onto planetary surfaces. Such showers may be indicated by the one to two orders of magnitude increase in accretion rate of L chondrite meteorites on Earth at ~500 Ma over a period of ~1 million years (Schmitz *et al*., 2003) and by moderate increases in the rates of large impacts on the terrestrial planets over the past ~100 million years. Proposed evidence for the latter includes the Chicxulub impact at the Cretaceous/Tertiary boundary on Earth (65 Ma) that may have resulted from disruption of a large asteroid ~100 million years earlier (Bottke *et al*., 2007).

Detailed observations of the surfaces of the satellites of the outer solar system planets of Jupiter, Saturn, Uranus, and Neptune were first made by flybys of the Voyager 1 and 2 spacecraft in the late 1970s. Those observations were supplemented by higher resolution imaging campaigns for the Galilean satellites (Io, Ganymede, Europa, and Callisto) of Jupiter by the Galileo mission to the Jovian system from 1995 to 2003. The Cassini mission first collected data of the Jovian system during a flyby in 2000–2001 and then entered the Saturnian system in 2004. These missions enabled study of the crater populations of the icy satellites. Additional complicating factors in using these crater populations include the relaxation of craters within the icy target materials (e.g., McKinnon *et al*., 1991; Schenk *et al*., 2004). Each body has its unique composition, thermal character, and resurfacing history that affect the cratering record. The crater size-frequency distributions of Ganymede, Callisto, and Europa show discrepancies from that of Earth's Moon, although the sources of the differences are uncertain (e.g., Schenk *et al*., 2004). These factors result in large uncertainties in modeling cratering rates for outer solar system bodies. Some sparsely cratered surfaces, such as those of Europa and large parts of Enceladus, appear to be geologically young due to resurfacing by eruption of volatiles, including plumes of gas and debris vented from the south pole of Enceladus as observed by the Cassini mission (Porco *et al*., 2006). In addition, if satellites are rotating synchronously with their orbiting of the Sun, their leading hemispheres are expected to be much more cratered than their leeward ones. However, the hemispheres of the more heavily cratered Ganymede and Callisto show little signature of such an asymmetry, indicating that they may have once rotated nonsynchronously (Schenk *et al*., 2004).

Controversy exists in how to interpret ages of outer solar system surfaces from the cratering record. One view is that modern sources of outer solar system projectiles, namely ecliptic comets, were also the sources of ancient impacts (Shoemaker and Wolfe, 1982). Ecliptic comets orbit near the plane of the ecliptic and thus have enhanced planetary interaction; they are thought to originate from the Kuiper belt (Duncan and Levison, 1997; Zahnle *et al*., 1998). In contrast, Neukum *et al*. (1998, 1999) suggested that the entire solar system was dominated by a single impactor population during heavy bombardment, such that large impact basins on Ganymede and Callisto date back to that time. This assumption leads to low impact rates, indicating that the surfaces date back to ancient times. These two scenarios lead to widely varying results for the Galilean satellites (Table 15.4). Farther out from Jupiter, uncertainties grow larger regarding the populations of impactors and sources that may also include broken-up satellites (e.g., McKinnon *et al*., 1991).

TABLE 15.4 Suggested Surface Ages for the Galilean Satellites of Jupiter.

Satellite	Suggested Surface age (Ma)	References
Io	2.3 to <0.3	Schenk *et al*. (2004), Zahnle *et al*. (2003)
Europa	10	Zahnle *et al*. (1998)
Europa	60	Zahnle *et al*. (2003)
Europa	3000 to 1000	Neukum *et al*. (1999)
Ganymede	700 (Gilgamesh) 2000 (bright terrains)	Zahnle *et al*. (2003)
Ganymede	3600 (bright terrains) 3800 (Gilgamesh) 4200 (dark terrains)	Neukum *et al*. (1998)
Callisto	2000 (Lofn and Valhalla impacts)	Zahnle *et al*. (2003)
Callisto	4300 to 3900 (various terrains and impacts)	Neukum *et al*. (1998), Wagner *et al*. (1999)

REFERENCES

Antonenko, I., Head III, J.W., Mustard, J.F., Hawke, B.R., 1995. Criteria for the detection of lunar cryptomaria. Earth, Moon and the Planets 69, 141–172.

Basaltic Volcanism Study Project, 1981. Basaltic Volcanism on the Terrestrial Planets. Lunar and Planetary Institute, Houston, p. 1286.

Basilevsky, A.T., Head, J.W., 1995. Global stratigraphy of Venus: Analysis of a random sample of thirty-six test areas. Earth, Moon, and the Planets 66, 285–366.

Basilevsky, A.T., Head, J.W., Schaber, G.G., Strom, R.G., 1997. The resurfacing history of Venus. In: Bougher, S.W., Hunten, D.M., Phillips, R.J. (Eds.), Venus II. The University of Arizona Press, Tucson, pp. 1047–1084.

Berman, D.C., Hartmann, W.K., 2002. Recent fluvial, volcanic, and tectonic activity on the Cerberus plains on Mars. Icarus 159, 1–17.

Bernatowicz, T.J., Hohenberg, C.M., Hudson, B., Kennedy, B.M., Podosek, F.A., 1978. Argon ages for lunar breccias 14064 and 15405. Proceedings of the Lunar Science Conference 9, 905–919.

Bibring, J.-P., Langevin, Y., Gendrin, A., Gondet, B., Poulet, F., Berthé, M., Soufflot, A., Arvidson, R., Mangold, N., Mustard, J., Drossart, P., and the OMEGA team, 2005. Mars surface diversity as revealed by the OMEGA/Mars Express observations. Science 307, 1576–1581.

Bogard, D.D., Garrison, D.H., Shih, C.-Y., Nyquist, L.E., 1994. ^{40}Ar-^{39}Ar dating of two lunar granites: The age of Copernicus. Geochimica et Cosmochimica Acta 58, 3093–3100.

Bottke, W.F., Vokrouhlicky, D., Nesvorny, D., 2007. An asteroid breakup 160 Myr ago as the probable source of the K/T impactor. Nature 449, 48–53.

Bouvier, A., Blichert-Toft, J., Vervoort, J.D., Albarède, F., 2005. The age of SNC meteorites and the antiquity of the Martian surface. Earth and Planetary Science Letters 240, 221–233.

Boyce, J.M., Dial Jr., A.L., 1975. Relative ages of flow units in Mare Imrium and Sinus Iridum. Proceedings of the Lunar Science Conference 6, 2585–2595.

Bullock, M.A., Grinspoon, D.H., 2001. The recent evolution of climate on Venus. Icarus 150, 19–37.

Burr, D.M., Grier, J.A., McEwen, A.S., Keszthelyi, L.P., 2002. Repeated aqueous flooding from the Cerberus Fossae: Evidence for very recently extant, deep groundwater on Mars. Icarus 159, 53–73.

Chapman, C.R., 1974. Cratering on Mars. I. Cratering and obliteration history. Icarus 22, 272–291.

Chapman, C.R., 1988. Mercury: Introduction to an end-member planet. In: Vilas, F., Chapman, C.R., Matthews, M.S. (Eds.), Mercury. The University of Arizona Press, Tucson, pp. 1–23.

Chapman, C.R., Pollack, J., Sagan, C., 1969. An analysis of the Mariner 4 photography of Mars. Astronomy Journal 74, 1039–1051.

Chapman, C.R., Ryan, E.V., Merline, W.J., Neukum, G., Wagner, R., Thomas, P.C., Veverka, J., Sullivan, R.J., 1996. Cratering on Ida. Icarus 120, 77–86.

Chapman, M.G., 2002. Layered, massive, and thin sediments on Mars: Possible Late Noachian to Late Amazonian tephra? In: Smellie, J.L., Chapman, M.G. (Eds.), Volcano-Ice Interactions on Earth and Mars. Geological Society Special Publications, 202, 273–203.

Chapman, M.G., Tanaka, K.L., 2002. Related magma-ice interactions: Possible origin for chasmata, chaos, and surface materials in Xanthe, Margaritifer, and Meridiani Terrae, Mars. Icarus 155, 2324–2339.

Chapman, M.G., Zimbelman, J.R., 1998. Coronae associations and their implications for Venus. Icarus 132, 344–361.

Christensen, P.R., Bandfield, J.L., Clark, R.N., Edgett, K.S., Hamilton, V.E., Hoefen, T., Kieffer, H.H., Kuzmin, R.O., Lane, M.D., Malin, C.V., Morris, R.V., Pearl, J.C., Pearson, R., Roush, T.L., Ruff, S.W., Smith, M.D., 2000a. Detection of crystalline hematite mineralization on Mars by the Thermal Emission Spectrometer: Evidence for near-surface water. Journal of Geophysical Research 105, 9623–9642.

Christensen, P.R., Bandfield, J.L., Smith, M.D., Hamilton, V.E., Clark, R.N., 2000b. Identification of a basaltic component on the Martian surface from Thermal Emission Spectrometer data. Journal of Geophysical Research 105, 9609–9621.

Connerney, J.E.P., Acuna, M.H., Wasilewski, P.J., Ness, N.F., Rème, H., Mazelle, C., Vignes, D., Lin, R.P., Mitchell, D.L., Cloutier, P.A., 1999. Magnetic lineations in the ancient crust of Mars. Science 284, 794–798.

Connerney, J.E.P., Acuna, M.H., Wasilewski, P.J., Kletetschka, G., Ness, N.F., Rème, H., Lin, R.P., Mitchell, D.L., 2001. The global magnetic field of Mars and implications for crustal evolution. Geophysical Research Letters 28, 4015–4018.

Craddock, R.A., Howard, A.D., 2002. The case for rainfall on a warm, wet early Mars. Journal of Geophysical Research 107 (E11), 5111. doi:10.1029/2001JE001505.

Crater Analysis Techniques Working Group, 1979. Standard techniques for presentation and analysis of crater size-frequency data. Icarus 37, 467–474.

Crown, D.A., Price, K.H., Greeley, R., 1992. Geologic evolution of the east rim of the Hellas basin, Mars. Icarus 100, 1–25.

Deutsch, A., Stöffler, D., 1987. Rb-Sr analyses of Apollo 16 melt rocks and a new age estimate for the Imbrium basin: Lunar basin chronology and the early heavy bombardment of the Moon. Geochimica et Cosmochimica Acta 51, 1951–1964.

Dohm, J.M., Tanaka, K.L., Hare, T.M., 2001. Geologic, paleotectonic, and paleoerosional maps of the Thaumasia region, Mars. US Geological Survey Geologic Investigations Series Map I-2650, scale, 1:5,000,000.

Duncan, M.J., Levison, H.F., 1997. A scattered comet disk and the origin of Jupiter family comets. Science 276, 1670–1672.

Fairén, A.G., Ruiz, J., Anguita, F., 2002. An origin for the linear magnetic anomalies on Mars through accretion of terranes: Implications for dynamo timing. Icarus 160, 220–223.

Fassett, C.I., Head III, J.W., 2008a. The timing of Martian valley network activity: Constraints from buffered crater counting. Icarus 195, 61–89.

Fassett, C.I., Head III, J.W., 2008b. Valley network-fed, open-basin lakes on Mars: Distribution and implications for Noachian surface and subsurface hydrology. Icarus 198, 37–56.

Frey, H.V., 2005. Impact constraints on the age and origin of the lowlands on Mars. Geophysical Research Letters 33, L08S02. doi:10.1029/2005GL024484.

Frey, H.V., 2006. Impact constraints on, and a chronology for, major events in early Mars history. Journal of Geophysical Research 111, E08S91. doi:10.1029/2005JE002449.

Frey, H.V., Roark, J.H., Shockey, K.M., Frey, E.L., Sakimoto, S.E.H., 2002. Ancient lowlands on Mars. Geophysical Research Letters 29, 1384. doi:10.1029/2001GL013832.

Fujiwara, A., Kawaguchi, J., Yeomans, K., Abe, M., Mukai, T., Okada, T., Saito, J., Yano, H., Yoshikawa, M., Scheeres, D.J., Barnouin-Jha, O., Cheng, A.F., Demura, H., Gaskell, R.W., Hirata, N., Ikeda, H., Kominato, T., Miyamoto, H., Nakamura, A.M., Nakamura, R., Sasaki, S., Uesugi, K., 2006. The rubble-pile asteroid Itokawa as observed by Hayabusa. Science 312, 1330–1334.

Fuller, R.R., Head III, J.W., 2002. Amazonis Planitia: The role of geologically recent volcanism and sedimentation in the formation of the smoothest plains on Mars. Journal of Geophysical Research 107, 5081. doi:1029/2002JE001842.

Gomes, R., Levison, H.F., Tsiganis, K., Morbidelli, A., 2005. Origin of the cataclysmic Late Heavy Bombardment period of the terrestrial planets. Nature 435, 466–469.

Grimm, R.E., Hess, P.C., 1997. The crust of Venus. In: Bougher, S.W., Hunten, D.M., Phillips, R.J. (Eds.), Venus II. The University of Arizona Press, Tucson, pp. 1205–1244.

Guest, J.E., Greeley, R., 1983. Geologic map of the Shakespeare quadrangle of Mercury. US Geological Survey Miscellaneous Investigations Series Map I-1408, scale 1:5,000,000.

Guest, J.E., Stofan, E.R., 1999. A new view of the stratigraphic history of Venus. Icarus 139, 55–66.

Haines, E.L., Metzger, A.E., 1980. Lunar highland crustal models based on iron concentrations: Isostasy and center-of-mass displacement. Proceedings of the Lunar and Planetary Science Conference 11, 689–718.

Hamilton, V.E., Stofan, E.R., 1996. The geomorphology and evolution of Hecate Chasma, Venus. Icarus 121, 171–194.

Hansen, V.L., 2000. Geologic mapping of tectonic planets. Earth and Planetary Science Letters 176, 527–542.

Hartmann, W.K., 1965. Terrestrial and lunar flux of large meteorites in the last two billion years. Icarus 4, 157–165.

Hartmann, W.K., 1967. Lunar crater counts I: Alphonsus. Communications of the Lunar and Planetary Laboratory 6, 31–38.

Hartmann, W.K., 1970. Lunar cratering chronology. Icarus 13, 209–301.

Hartmann, W.K., 1971. Martian cratering III: Theory of crater obliteration. Icarus 15, 410–428.

Hartmann, W.K., 1972. Paleocratering of the Moon: Review of post-Apollo data. Astrophysics and Space Science 12, 48–61.

Hartmann, W.K., 1973. Martian cratering, 4, Mariner 9 initial analysis of cratering chronology. Journal of Geophysical Research 78, 4096–4116.

Hartmann, W.K., 2003. Megaregolith evolution and cratering cataclysm models–Lunar cataclysm as a misconception (28 years later). Meteoritics & Planetary Science 38, 579–593.

Hartmann, W.K., 2005. Martian cratering 8: Isochron refinement and the chronology of Mars. Icarus 174, 294–320.

Hartmann, W.K., 2007. Martian chronology: Toward resolution of the 2005 "controversy" and evidence for obliquity-driven resurfacing processes. Seventh International Conference on Mars Houston: Lunar and Planetary Institute, Abstract on CD-ROM, #3318.

Hartmann, W.K., Neukum, G., 2001. Cratering chronology and the evolution of Mars. Space Science Reviews 96, 165–194.

Hartmann, W.K., Neukum, G., Werner, S., 2007. Confirmation and utilization of the "production function" size-frequency distributions of Martian impact craters. Geophysical Research Letters 35, L02205. doi:10.1029/2007GL031557.

Hauck II, S.A., Phillips, R.J., Price, M.H., 1998. Venus: Crater distribution and plains resurfacing models. Journal of Geophysical Research 103, 13635–13642.

Hawke, B.R., Bell, J.F., 1981. Remote sensing studies of lunar dark-halo impact craters: Preliminary results and implications of early volcanism. Proceedings of the Lunar and Planetary Science Conference 12B, 665–678.

Hiesinger, H., Head III, J.W., Wolf, U., Jaumann, R., Neukum, G., 2003. Ages and stratigraphy of mare basalts in Oceanus Precellarum, Mare Nubium, Mare Cognitum, and Mare Insularum. Journal of Geophysical Research 108, 5065. doi:10.1029/2002JE001985.

Hubbard, N.J., Meyer Jr., C., Gast, P.W., Wiesmann, H., 1971. The composition and derivation of Apollo 12 soils. Earth and Planetary Science Letters 10, 341–350.

Hynek, B.M., Phillips, R.J., Arvidson, R.E., 2003. Explosive volcanism in the Tharsis region: Global evidence in the Martian geologic record. Journal of Geophysical Research 108, 5111. doi:10.1029/2003JE002062.

Irwin III, R.P., Maxwell, T.A., Howard, A.D., Craddock, R.A., Leverington, D.W., 2002. A large paleolake basin at the head of Ma'adim Vallis, Mars. Science 296, 2209–2212.

Irwin III, R.P., Howard, A.D., Craddock, R.A., Moore, J.M., 2005. An intense terminal epoch of widespread fluvial activity on early Mars: 2. Increased runoff and paleolake development. Journal of Geophysical Research 110, E12S15. doi:10.1029/2005JE002460.

Ivanov, B.A., 2001. Mars/Moon cratering rate ratio estimates. Space Science Reviews 96, 87–104.

Jedicke, R., Metcalfe, T.S., 1998. The orbital and absolute magnitude distributions of main belt asteroids. Icarus 131, 245–260.

Keszthelyi, L., McEwen, A.S., Thordarson, T., 2000. Terrestrial analogs and thermal models for Martian flood lavas. Journal of Geophysical Research 105, 15027–15050.

Kreslavsky, M.A., Head, J.W., 2000. Kilometer-scale roughness of Mars: Results from MOLA data analysis. Journal of Geophysical Research 105, 26695–26711.

Kreslavsky, M.A., Head, J.W., 2002. Fate of outflow channel effluents in the northern lowlands of Mars: The Vastitas Borealis Formation as a sublimation residue from frozen ponded bodies of water. Journal of Geophysical Research 107, 5121. doi:10.1029/2001JE001831.

Leake, M.A., Chapman, C.R., Weidenschilling, S.J., Davis, D.R., Greenberg, R., 1987. The chronology of Mercury's geological and geophysical evolution: The vulcanoid hypothesis. Icarus 71, 350–375.

Leonard, G.J., Tanaka, K.L., 2001. Geologic map of the Hellas region of Mars. US Geological Survey Geologic Investigations Series Maps I-2694, scale 1:5,000,000.

Levison, H.F., Dones, L., Chapman, C.R., Stern, S.A., Duncan, M.J., Zahnle, K., 2001. Could the lunar "Late Heavy Bombardment" have been triggered by the formation of Uranus and Neptune? Icarus 151, 286–306.

Liou, J.-C., Malhotra, R., 1997. Depletion of the outer asteroid belt. Science 275, 375–377.

Malin, M.C., Edgett, K.S., 2000. Sedimentary rocks of early Mars. Science 290, 1927–1937.

Malin, M.C., Edgett, K.S., 2001. Mars Global Surveyor Mars Orbiter Camera–interplanetary cruise through primary mission. Journal of Geophysical Research 106, 23429–24570.

Malin, M.C., Edgett, K.S., 2003. Evidence for persistent flow and aqueous sedimentation on early Mars. Science 302, 1931–1934.

Malin, M.C., Edgett, K.S., Posiolova, L.V., McColley, S.M., Noe Dobrea, E.Z., 2006. Present-day impact cratering rate and contemporary gully activity on Mars. Science 314, 1573–1577.

McCauley, J.F., Guest, J.E., Schaber, G.G., Trask, N.J., Greeley, R., 1981. Stratigraphy of the Caloris basin, Mercury. Icarus 47, 184–202.

McEwen, A.S., Malin, M.C., Carr, M.H., Hartmann, W.K., 1999. Voluminous volcanism on early Mars revealed in Valles Marineris. Nature 397, 584–586.

McEwen, A.S., Preblich, B.S., Turtle, E.P., Artemieva, N.A., Golombek, M.P., Hurst, M., Kirk, R.L., Burr, D.M., Christensen, P.R., 2005. The rayed crater Zunil and interpretations of small impact craters on Mars. Icarus 176, 351–381.

McKay, G.A., Wiesmann, H., Bansal, J.L., Shih, C.-Y., 1979. Petrology, chemistry, and chronology of Apollo 14 KREEP basalts. Proceedings of the Lunar and Planetary Science Conference 10, 181–205.

McKinnon, W.B., Chapman, C.R., Housen, K.R., 1991. Cratering of the Uranian satellites. In: Bergstralh, J.T., Miner, E.D., Matthews, M.S. (Eds.), Uranus. The University of Arizona Press, Tucson, pp. 629–692.

McKinnon, W.B., Zahnle, K.J., Ivanov, B.A., Melosh, H.J., 1997. Cratering on Venus: Models and observations. In: Bougher, S.W., Hunten, D.M., Phillips, R.J. (Eds.), Venus II. The University of Arizona Press, Tucson, pp. 1047–1084.

Melosh, H.J., 1989. Impact Cratering: A Geologic Process. Oxford University Press, New York, p. 245.

Moore, J.M., Wilhelms, D.E., 2001. Hellas as a possible site of ancient ice-covered lakes on Mars. Icarus 154, 258–276.

Namiki, N., Solomon, S.C., 1994. Impact crater densities on volcanoes and coronae on Venus: Implications for volcanic resurfacing. Science 265, 929–933.

Neukum, G., Ivanov, B.A., 1994. Crater size distributions and impact probabilities on Earth from lunar, terrestrial-planet, and asteroid cratering data. In: Gehrels, T. (Ed.), Hazards Due to Comets & Asteroids. The University of Arizona Press, Tucson, pp. 359–416.

Neukum, G., Wise, D.U., 1976. Mars: A standard crater curve and possible new time scale. Science 194, 1381–1387.

Neukum, G., Wagner, R., Wolf, U., Ivanov, B.A., Head III, J.W., Pappalardo, R.T., Klemaszewski, J.E., Greeley, R., Belton, M.J.S., and the Galileo SSI Team, 1998. Cratering chronology in the Jovian system and derivation of absolute ages. 29th Annual Lunar and Planetary Science Conference Houston, March 16–20, Abstract on CD-ROM, 1742.

Neukum, G., Wagner, R., Wolf, U., and the Galileo SSI Team, 1999. Cratering record of Europa and implications for timescale and crustal development. 29th Annual Lunar and Planetary Science Conference Houston, March 16–20, Abstract on CD-ROM, 1992.

Neukum, G., Ivanov, B.A., Hartmann, W.K., 2001. Cratering records in the inner solar system in relation to the lunar reference system. Space Science Reviews 96, 55–86.

Nimmo, F., Tanaka, K., 2005. Early crustal evolution of Mars. Annual Reviews of Earth and Planetary Science 33, 133–161.

Nyquist, L.E., Bogard, D.D., Shish, C.-Y., Greshake, A., Stöffler, D., Eugster, O., 2001. Ages and geologic histories of Martian meteorites. Space Science Reviews 96, 105–164.

Parker, T.J., Saunders, R.S., Schneeberger, D.M., 1989. Transitional morphology in west Deuteronilus Mensae, Mars: Implications for modification of the lowland/upland boundary. Icarus 82, 111–145.

Phillips, R.J., Zuber, M.T., Solomon, S.C., Golombek, M.P., Jakosky, B.M., Banerdt, W.B., Smith, D.E., Williams, R.M.E., Hynek, B.M., Aharonson, O., Hauck, S.A., 2001. Ancient geodynamics and global-scale hydrology on Mars. Science 291, 2587–2591.

Plaut, J.J., Picardi, G., Safaeiniti, A., Ivanov, A.B., Milkovich, S.M., Cicchetti, A., Kofman, W., Mouginot, J., Farrell, W.M., Phillips, R.J., Clifford, S.M., Frigeri, A., Orosei, R., Federico, C., Williams, I.P., Gurnett, D.A., Nielsen, E., Hagfors, T., Heggy, E., Stofan, E.R., Plettemeier, D., Watters, T.R., Leuschen, C.J., Edenhofer, P., 2007. Subsurface radar sounding of the south polar layered deposits of Mars. Science 316, 92–95.

Plescia, J.B., 2003. Cerberus Fossae, Elysium, Mars: A source for lava and water. Icarus 164, 79–95.

Porco, C.C., Helfenstein, P., Thomas, P.C., Ingersoll, A.P., Wisdom, J., West, R., Neukum, G., Denk, T., Wagner, R., Roatsch, T., Kieffer, S., Turtle, E., McEwen, A., Johnson, T.V., Rathbun, J., Veverka, J., Wilson, D., Perry, J., Spitale, J., Brahic, A., Burns, J.A., Del Genio, A.D., Dones, L., Murray, C.D., Squyres, S., 2006. Cassini observes the active south pole of Enceladus. Science 311, 1393–1401.

Price, M., Suppe, J., 1995. Constraints on the resurfacing history of Venus from the hypsometry and distribution of volcanism, tectonism, and impact craters. Earth, Moon, and Planets 71, 99–145.

Price, M.H., Watson, G., Suppe, J., Brankman, C., 1996. Dating volcanism and rifting on Venus using impact crater densities. Journal of Geophysical Research 101, 4657–4671.

Prinz, M., Keil, K., 1977. Mineralogy, petrology and chemistry of ANT-suite rocks from the lunar highlands. Physics and Chemistry of the Earth 10, 215–237.

Ryder, G., Bogard, D.D., Garrison, D., 1991. Probable age of Autolycus and calibration of lunar stratigraphy. Geology 19, 143–146.

Schaber, G.G., McCauley, J.F., 1980. Geological map of the Tolstoj quadrangle of Mercury (H-8). US Geological Survey Miscellaneous Investigations Series Map I-1199, scale 1:5,000,000.

Schenk, P.M., Chapman, C.R., Zahnle, K., Moore, J.M., 2004. Ages and interiors: The cratering record of the Galilean satellites. In: Bagenal, F., Dowling, T.E., McKinnon, W.B. (Eds.), Jupiter: The Planet, Satellites and Magnetosphere. Cambridge University Press, Cambridge, pp. 427–456.

Schmitz, B., Peucker-Ehrenbrink, B., Lindström, M., Tassinari, M., 2003. Accretion rates of meteorites and cosmic dust in the Early Ordivician. Science 278, 88–90.

Schultz, P.H., Gault, D.E., 1975. Seismic effects from major basin formation on the Moon and Mercury. The Moon 12, 159–177.

Schultz, P.H., Spudis, P.D., 1979. Evidence for ancient mare volcanism. Proceedings of the Lunar and Planetary Science Conference 10, 2899–2918.

Scott, D.H., Carr, M.H., 1978. Geologic map of Mars. US Geological Survey Miscellaneous Investigations Series Map I-1083, scale 1:25,000,000.

Scott, D.H., Tanaka, K.L., 1981. Mars: Paleostratigraphic restoration of buried surfaces in Tharsis Montes. Icarus 45, 304–319.

Scott, D.H., Tanaka, K.L., 1982. Ignimbrites of Amazonis Planitia region of Mars. Journal of Geophysical Research 87, 1179–1190.

Scott, D.H., Greeley, R., Guest, J.E., Tanaka, K.L., 1986–87. Geologic maps of the western and eastern equatorial and polar regions of Mars. US Geological Survey Miscellaneous Investigations Series Maps I-1802-A, B, C, scale 1:15,000,000.

Shoemaker, E.M., Hackman, R.J., 1962. Stratigraphic basis for a lunar time scale. In: Kopal, Z., Mikhailov, Z.K. (Eds.), The Moon. Academic Press, London, pp. 289–300.

Shoemaker, E.M., Wolfe, R.F., 1982. Cratering time scales for the Galilean satellites. In: Morrison, D. (Ed.), Satellites of Jupiter. The University of Arizona Press, Tucson, pp. 277–339.

Skinner Jr., J.A., Tanaka, K.L., 2007. Evidence for and implications of sedimentary diapirism and mud volcanism in the southern Utopia highland-lowland boundary plains, Mars. Icarus 186, 41–59.

Smith, D.E., Zuber, M.T., Solomon, S.C., Phillips, R.J., Head, J.W., Garvin, J.B., Banerdt, W.B., Muhleman, D.O., Pettengill, G.H., Neumann, G.A., Lemoine, F.G., Abshire, J.B., Aharonson, O., Brown, C.D., Hauck, S.A., Ivanov, A.B., McGovern, P.J., Zwally, H.J., Duxbury, T.C., 1999. The global topography of Mars and implications for surface evolution. Science 284, 1495–1503.

Soderblom, L.A., Lebofsky, L.A., 1972. Technique for rapid determination of relative ages of lunar areas from orbital photography. Journal of Geophysical Research 77, 279–296.

Soderblom, L.A., Condit, C.D., West, R.A., Herman, B.M., Kriedler, T.J., 1974. Martian planetwide crater distributions: Implications for geologic history and surface processes. Icarus 22, 239–263.

Solomon, S.C., Bullock, M.A., Grinspoon, D.H., 1999. Climate change as a regulator of tectonics on Venus. Science 286, 87–90.

Spudis, P.B., 1985. A mercurian chronostratigraphic classification. Reports of the Planetary Geology and Geophysics Program, NASA. Technical Memorandum 87563, 595–597.

Spudis, P.D., Guest, J.E., 1988. Stratigraphy and geologic history of Mercury. In: Vilas, F., Chapman, C.R., Matthews, M.S. (Eds.), Mercury. The University of Arizona Press, Tucson, pp. 118–164.

Stöffler, D., Ryder, G., 2001. Stratigraphy and isotope ages of lunar geologic units: Chronological standard for the inner solar system. Space Science Reviews 96, 9–54.

Stöffler, D., Bischoff, A., Borchardt, R., Burghele, A., Deutsch, A., Jessberger, E.K., Ostertag, R., Palme, H., Spettel, B., Reimold, W.U., Wacker, K., Wanke, H., 1985. Composition and evolution of the lunar crust in the Descartes highlands, Apollo 16. Journal of Geophysical Research 89, 449–506.

Strom, R.G., 1977. Origin and relative age of lunar and mercurian intercrater plains. Physics of the Earth and Planetary Interiors 15, 156–172.

Strom, R.G., Neukum, G., 1988. The cratering record on Mercury and the origin of impacting objects. In: Vilas, F., Chapman, C.R., Matthews, M.S. (Eds.), Mercury. The University of Arizona Press, Tucson, pp. 336–373.

Strom, R.G., Schaber, G.G., Dawson, D.D., 1994. The global resurfacing of Venus. Journal of Geophysical Research 99, 10899–10926.

Strom, R.G., Malhotra, R., Ito, T., Yoshida, F., Kring, D.A., 2005. The origin of planetary impactors in the inner solar system. Science 309, 1847–1850.

Stuart-Alexander, D.E., Wilhelms, D.E., 1975. The Nectarian System, a new lunar time-stratigraphic unit. US Geological Survey Journal of Research 3, 53–58.

Tanaka, K.L., 1986. The stratigraphy of Mars. Proceedings of the Lunar and Planetary Science Conference 17, part 1. Journal of Geophysical Research 91, E139–E158.

Tanaka, K.L., Kolb, E.J., 2001. Geologic history of the polar regions of Mars based on Mars Global Surveyor Data: I. Noachian and Hesperian Periods. Icarus 154, 3–21.

Tanaka, K.L., Leonard, G.J., 1995. Geology and landscape evolution of the Hellas region of Mars. Journal of Geophysical Research 100, 5407–5432.

Tanaka, K.L., Isbell, N.K., Scott, D.H., Greeley, Ronald, Guest, J.E., 1988. The resurfacing history of Mars: A synthesis of digitized, Viking-based geology. Proceedings of the Lunar and Planetary Science Conference 18, 665–678.

Tanaka, K.L., Dohm, J.M., Lias, J.H., Hare, T.M., 1998. Erosional valleys in the Thaumasia region of Mars–Hydrothermal and seismic origins. Journal of Geophysical Research 103, 31407–31419.

Tanaka, K.L., Banerdt, W.B., Kargel, J.S., Hoffman, N., 2001. Huge, CO_2-charged debris-flow deposit and tectonic sagging in the northern plains of Mars. Geology 29, 427–430.

Tanaka, K.L., Skinner Jr., J.A., Hare, T.M., Joyal, T., Wenker, A., 2003. Resurfacing history of the northern plains of Mars based on geologic mapping of Mars Global Surveyor data. Journal of Geophysical Research 108, 8043. doi:10.1029/2002JE001908.

Tanaka, K.L., Skinner Jr., J.A., Hare, T.M., 2005. Geologic map of the northern plains of Mars. US Geological Survey Scientific Investigations Map SIM-2888, scale 1:15,000,000.

Tanaka, K.L., Skinner Jr., J.A., Barlow, N.G., 2006. How geology affects crater size-frequency distributions and determinations of the crater production function for craters >5 km in diameter on Mars. Workshop on Surface Ages and Histories: Issues in Planetary Chronology. Houston, May 21–23, Abstract on CD-ROM, #6014.

Taylor, S.R., 1975. Lunar Science: A Post-Apollo View. Pergamon, New York, p. 372.

Taylor, S.R., 1982. Planetary Science: A Lunar Perspective. Lunar and Planetary Institute, Houston, p. 481.

Tsiganis, K., Gomes, R., Morbidelli, A., Levison, H.F., 2005. Origin of the orbital architecture of the giant planets of the Solar System. Nature 435, 459–461.

Turner, G., Cadogan, P.H., Yonge, C.J., 1973. Argon selenochronology. Proceedings of the Lunar Science Conference 4, 1889–1914.

Veverka, J., Thomas, P., Harch, A., Clark, B., Bell, J.F., Carcich, B., Joseph, J., Chapman, C., Merline, W., Robinson, M., Malin, M., McFadden, L.A., Murchie, S., Hawkins, S.E., Farquhar, R., Izenberg, N., Cheng, A., 1997. NEAR's flyby of 253 Mathilde: Images of a C asteroid. Science 278, 2109–2114.

Wagner, R., Wolf, U., Neukum, G., and the Galileo SSI Team, 1999. Ages of individual craters on the Galilean satellites Ganymede and Callisto. 30th Lunar and Planetary Science Conference Houston, March 15–19, Abstract on CD-ROM, #1818.

Walker, D., Longhi, J., Hays, J.F., 1975. Differentiation of a very thick magma body and implications for the source regions of mare basalts. Proceedings of the Lunar Science Conference 6, 1103–1120.

Werner, S.C., 2006. Major Aspects of the Chronostratigraphy and Geologic Evolutionary History of Mars. Cuvillier Verlag, Göttingen, p. 160 [reprinted PhD thesis, Berlin, Freien Universität, 2005].

Werner, S.C., 2008. The early martian evolution–constraints from basin formation ages. Icarus 195, 45–60.

Werner, S.C., Tanaka, K.L., 2011. Redefinition of the crater-density and absolute-age boundaries for the chronostratigraphic system of Mars. Icarus 215 (2), 603–607.

Werner, S.C., Tanaka, K.L., Skinner Jr., J.A., 2011. Mars: The evolutionary history of the northern lowlands based on crater counting and geologic mapping. Planetary and Space Science 59, 1143–1165.

Whiteley, R.J., Tholen, D.J., Hergenrother, C.W., 2002. Lightcurve analysis of four new monolithic fast-rotating asteroids. Icarus 157, 139–154.

Wilhelms, D.E., 1980. Stratigraphy of part of the lunar nearside. US Geological Survey Professional Paper 1046-A, A1–A71.

Wilhelms, D.E., 1987. The geologic history of the Moon. US Geological Survey Professional Paper 1348, 302.

Wilhelms, D.E., Baldwin, R.J., 1989. The role of igneous sills in shaping the Martian uplands. Proceedings of the Lunar and Planetary Science Conference 19, 355–365.

Wilhelms, D.E., McCauley, J.F., 1971. Geologic map of the nearside of the Moon. US Geological Survey Map I-703, scale 1:5,000,000.

Wilhelms, D.E., Oberbeck, V.R., Aggarwal, H.R., 1978. Size-frequency distributions of primary and secondary lunar impact craters. Proceedings of the Lunar and Planetary Science Conference 9, 3735–3762.

Witbeck, N.E., Tanaka, K.L., Scott, D.H., 1991. Geologic map of the Valles Marineris region, Mars. US Geological Survey Miscellaneous Investigations Series Map I-2010, scale 1:2,000,000.

Yoshida, F., Nakamura, T., 2004. Basic nature of sub-km main-belt asteroids: Their size and spatial distributions. Advances in Space Research 33, 1543–1547.

Zahnle, K., Dones, L., Levison, H.F., 1998. Cratering rates on the Galilean satellites. Icarus 153, 111–129.

Zahnle, K., Schenk, P., Levison, H., Dones, L., 2003. Cratering rates in the outer solar system. Icarus 163, 263–289.